

Orbital Wigner functions and quantum transport in multiband systems

Johannes Mitscherling,^{1,2,*} Dan S. Borgnia,^{2,*} SuryaNeil Ahuja,² Joel E. Moore,^{2,3} and Vir B. Bulchandani⁴

¹*Max Planck Institute for the Physics of Complex Systems, Nöthnitzer Str. 38, 01187 Dresden, Germany*

²*Department of Physics, University of California, Berkeley, CA 94720, USA*

³*Materials Sciences Division, Lawrence Berkeley National Laboratory, Berkeley, CA 94720, USA*

⁴*Department of Physics and Astronomy, Rice University, 6100 Main Street Houston, TX 77005, USA*

Traditional theories of electron transport in crystals are based on the Boltzmann equation and do not capture physics arising from quantum coherence. We introduce a transport formalism based on “orbital Wigner functions”, which accurately captures quantum coherent physics in multiband fermionic systems. We illustrate the power of this approach compared to traditional semiclassical transport theory by testing it numerically against microscopic simulations of one-dimensional, non-interacting, two-band systems — the simplest systems capable of exhibiting inter-orbital coherence. We show that orbital Wigner functions accurately capture strongly non-equilibrium features of electron dynamics that lie beyond conventional Boltzmann theory, such as the ballistic transport of a relative phase between microscopic orbitals and topological Thouless pumping of charge both at non-zero temperature and away from the adiabatic limit. Our approach is motivated in part by modern ultracold atom experiments that can prepare and measure far-from-equilibrium charge transport and phase coherence in multiband fermionic systems, calling for correspondingly precise theories of transport. The quantitative accuracy exhibited by our approach, together with its capacity to capture nontrivial physics even at the ballistic scale, establishes orbital Wigner functions as an ideal starting point for developing a fully systematic theory of transport in crystals.

I. INTRODUCTION

A. Background and motivation

The semiclassical theory of electron transport in crystals has changed little since its development by Drude, Sommerfeld and others in the early part of the previous century. Perhaps its most significant revision was the inclusion of Berry-curvature effects such as the Karplus-Luttinger anomalous velocity [1–3], many decades after the anomalous velocity was discovered [4], culminating in a successful theory of the anomalous Hall effect [5–7]. It seems remarkable in hindsight that such an essential feature of electron transport was missed for so long. One possible explanation for this delay is the well-known lack of a fully systematic derivation of the semiclassical equations of motion for electron transport, despite their traditional justification from wavepackets of Bloch electrons [8]. Nevertheless, a suitably careful analysis of such Bloch-electron wavepackets turned out to be sufficient to capture Berry-curvature effects [1–3], and the resulting equations of motion form the bedrock of the modern theory of transport.

Despite correctly accounting for Berry-curvature effects, semiclassical transport theory is less reliable above zero temperature and in the presence of multiple bands. In particular, quantum coherences between different single-particle bands become possible, whose accurate description requires a matrix-valued transport equation rather than “one Boltzmann equation per band” as arises when quantum coherences are neglected [8]. Systematic

approaches to quantum transport in multiband systems range from analyses using the non-Abelian Berry curvature in the special case of degenerate or near-degenerate bands [9–11], to more general Wigner-function based approaches [12–25] that model time evolution of the full single-particle density matrix and not just its diagonal elements as tradition dictates.

Such Wigner-function based approaches to quasiparticle transport have a long history in physics, starting from the pioneering work of Irving and Zwanzig in 1951 [26]. However, they have only been applied to electrons in crystal lattices more recently, with two notable strands of work in this area. One popular approach in solid-state physics (see Refs. [12–25] and references therein) consists of deriving dynamical equations for Wigner functions of Bloch electrons. While this approach has yielded numerous qualitative physical insights, it is not well suited to quantitative tests of its validity because the position-space marginals of the resulting Wigner functions bear little resemblance to the physical carrier density in general, unless the position variables are corrected in a non-trivial fashion [14, 18]. In fact, the first rigorous definition of a Wigner function on the lattice with the correct position-space marginals was obtained in 2012 by Hinarejos, Pérez and Bañuls [27]. While this development appears to have escaped notice in most literature on Bloch-electron transport, this alternative approach was pursued further in the setting of one-dimensional systems, where it now forms the basis of a quantitatively accurate and thoroughly tested theory of transport [28–32].

Our paper seeks to bridge this gulf between the richness of multiband transport in arbitrary crystal lattices and the rigour of recent approaches to transport in one dimension. We achieve this by proposing “orbital Wigner functions” as an alternative to previous

* These authors contributed equally.

Bloch-electron-based constructions of Wigner functions in crystal lattices. Such orbital Wigner functions satisfy the crucial consistency property identified by Hinarejos et al. [27, 33], which we view as a prerequisite for obtaining quantitatively accurate predictions for the space-time electron density. We benchmark our proposed transport equation against microscopic numerical simulations of the simplest non-trivial case, namely one-dimensional, non-interacting, two-band systems.

Even in this apparently simple setting, which involves only “streaming” rather than “collision” terms in the Boltzmann language, we identify physical effects that fall beyond the purview of textbook transport theory, such as time evolution from locally thermal states perturbed by a coherent interorbital phase, or Thouless-type [34] charge pumping that persists both far from adiabaticity and at non-zero temperature. We nevertheless show in all such cases that the resulting charge and current dynamics is captured to within numerical accuracy by our proposed ballistic-scale transport equation. At the same time, we present numerical evidence and a general analytical argument that our proposed equation recovers standard Boltzmann-theory predictions in local thermal equilibrium, and therefore does not contradict the textbook understanding of electron transport [8]. We note that the stringent benchmarking procedure that we follow in this work is applicable in principle to any other proposed transport equation for electrons in crystal lattices, and may thus be of independent interest.

The reader might wonder at our emphasis on quantitative accuracy, given that the theory of transport in crystals is often viewed as a coarse-grained and largely qualitative tool. Our motivations are two-fold. First, contemporary ultracold atom experiments are capable of imaging spacetime profiles of conserved charge densities in mesoscopic systems with sufficient accuracy to discern their lineshapes [35–41], and therefore demand similarly quantitatively accurate theoretical predictions. Second, all the difficulties of transport theory are usually held to lie in its collision terms, whose derivation relies on uncontrolled approximations such as Boltzmann’s long-controversial molecular chaos assumption. The fact that multiband systems exhibit nontrivial physics at the level of their streaming terms indicates that more care is needed to capture quantum coherent effects, even at the ballistic or Euler scale [42] where dissipative corrections can be ignored.

B. Guide to results

We introduce a transport theory based on orbital Wigner functions for generic tight-binding Hamiltonians on d -dimensional crystal lattices in Section II. The matrix-valued orbital Wigner function $w(\mathbf{x}, \mathbf{k})$ defined in Eq. (12) allows us to capture local densities of conserved operators, such as the local charge density and local charge-current density, even when the initial state is far

from equilibrium and quantum coherent. Starting from the exact Heisenberg equations of motion for fermion bilinears, we derive a coupled system of linear partial differential equations that captures the ballistic-scale dynamics of the orbital Wigner function, see Eq. (21). Our framework generalizes straightforwardly to time-dependent tight-binding Hamiltonians and external electrostatic potentials, see Eqs. (35) and (39) respectively.

We check the validity of our proposed transport equation against numerical free-fermion simulations in Sections III and IV for some representative Hamiltonians, parameter regimes, and initial states that lie beyond the scope of semiclassical transport theory. For example, we demonstrate that our transport equation accurately captures dynamics resulting from initial states with spatially-inhomogeneous single-particle coherence (Fig. 2), coherently driven Hamiltonians even for fast driving frequencies (Fig. 3), and the charge dynamics in topological Thouless pumps over multiple pumping cycles and far from the idealized adiabatic limit (Figs. 4 and 5), despite reducing to conventional Boltzmann theory in local thermal equilibrium as expected (Fig. 1). We also model stroboscopically driven Su-Schrieffer-Heeger (SSH) chains whose Bloch bands are always instantaneously flat, but nevertheless allow for far-from-equilibrium charge transport that is captured by our formalism (Fig. 6). Our results thus provide a unified starting point for making quantitative predictions about multiband dynamics and transport in state-of-the-art analogue quantum simulators and in advanced experiments on quantum materials, in far-from-equilibrium regimes that lie well beyond standard theoretical simplifications.

We close in Section V with a discussion of the possibilities opened up by our approach, which range from a systematic treatment of Berry curvature and further quantum geometric effects for multiple bands away from zero temperature, to natural extensions of our transport equation to include disorder or interactions, for example, through novel collision terms that correctly account for quantum coherence in multiband systems.

II. ORBITAL WIGNER FUNCTIONS

A. Hamiltonian conventions

We begin by fixing conventions for the fermionic tight-binding Hamiltonians that we will consider in this work, and their associated densities of charge, charge current and energy.

1. Tight-binding Hamiltonians

Let the index $j \in \Lambda$ label the sites $\mathbf{R}_j \in \mathbb{R}^d$ of a d -dimensional Bravais lattice and let τ_α denote the positions of additional degrees of freedom relative to \mathbf{R}_j

within each unit cell, with $\alpha = 1, 2, \dots, M$. The latter may reflect spin states, atomic orbitals, or other basis sites, all of which we refer to as ‘‘orbitals’’ for simplicity. Throughout the paper we set $\hbar = 1$ for convenience.

It will be useful to write $\mathbf{R}_{j\alpha} = \mathbf{R}_j + \boldsymbol{\tau}_\alpha$ for the absolute position of each orbital. A generic tight-binding Hamiltonian \hat{H}_0 associated with this crystal structure can be written as

$$\hat{H}_0 = - \sum_{j,j' \in \Lambda} \sum_{\alpha,\beta=1}^M t_{jj'}^{\alpha\beta} \hat{c}_{j\alpha}^\dagger \hat{c}_{j'\beta}. \quad (1)$$

We will assume lattice translation invariance, so that the hopping amplitudes depend only on the relative positions, $t_{jj'}^{\alpha\beta} = t_{\alpha\beta}(\mathbf{R}_j - \mathbf{R}_{j'})$. We also assume Hermiticity of the Hamiltonian, $t_{jj'}^{\alpha\beta} = (t_{j'j}^{\beta\alpha})^*$. For simplicity, we consider only finite-range hopping. Note that this Hamiltonian conserves the total charge $\hat{N} = \sum_{j \in \Lambda} \sum_{\alpha=1}^M \hat{c}_{j\alpha}^\dagger \hat{c}_{j\alpha}$. Eq. (1) represents the most general charge-conserving and non-interacting Hamiltonian for fermions arranged in a crystal lattice, and in particular, makes no additional assumptions about the underlying Wannier states that give rise to the tight-binding parameters $t_{jj'}^{\alpha\beta}$.

However, at various points in this paper, we will make the additional (albeit standard) assumption that the position of a given Wannier orbital is well-approximated by the position of its Wannier center. In particular, we make this assumption implicitly in Eq. (8) when defining the center-of-charge operator and its associated charge-current operator, and again in Eq. (36) when considering dynamics in external electrostatic fields. While these simplifying approximations should not affect our predictions at linear order in applied electric fields, nonlinear optical responses are particularly sensitive to such off-diagonal contributions to the center-of-charge or position operator [43–45].

2. Orbital versus Bloch electrons

We define momentum space fermions by

$$\hat{c}_\alpha(\mathbf{k}) = \sum_{j \in \Lambda} e^{-i\mathbf{k} \cdot \mathbf{R}_{j\alpha}} \hat{c}_{j\alpha} \quad (2)$$

(see Appendix A for a summary of our Fourier transform conventions), in terms of which

$$\hat{H}_0 = \int_{\text{BZ}} \frac{d\mathbf{k}}{V_{\text{BZ}}} \sum_{\alpha,\beta=1}^M h_{\alpha\beta}(\mathbf{k}) \hat{c}_\alpha^\dagger(\mathbf{k}) \hat{c}_\beta(\mathbf{k}), \quad (3)$$

where \int_{BZ} denotes integration over the first Brillouin zone with volume V_{BZ} , and the Bloch Hamiltonian $h_{\alpha\beta}(\mathbf{k}) = - \sum_{j \in \Lambda} t_{\alpha\beta}(\mathbf{R}_j) e^{-i\mathbf{k} \cdot (\mathbf{R}_j + \boldsymbol{\tau}_\alpha - \boldsymbol{\tau}_\beta)}$. For each \mathbf{k} , there exists an M -by- M unitary matrix $U(\mathbf{k})$ diagonalizing the matrix $h(\mathbf{k})$ such that

$$\sum_{\alpha,\beta=1}^M U_{m\alpha}^\dagger(\mathbf{k}) h_{\alpha\beta}(\mathbf{k}) U_{\beta n}(\mathbf{k}) = E_n(\mathbf{k}) \delta_{mn}, \quad (4)$$

which defines M energy bands $\{E_n(\mathbf{k})\}_{n=1}^M$ and Bloch electron creation operators $\hat{d}_n^\dagger(\mathbf{k}) := \sum_{\alpha=1}^M U_{\alpha n}(\mathbf{k}) \hat{c}_\alpha^\dagger(\mathbf{k})$, in terms of which

$$\hat{H}_0 = \int_{\text{BZ}} \frac{d\mathbf{k}}{V_{\text{BZ}}} \sum_{n=1}^M E_n(\mathbf{k}) \hat{d}_n^\dagger(\mathbf{k}) \hat{d}_n(\mathbf{k}). \quad (5)$$

We will refer to the excitations created by \hat{c}_α^\dagger and \hat{d}_n^\dagger as *orbital electrons* and *Bloch electrons* respectively.

3. Operator densities of conserved charges

It will be useful to define local Hamiltonian and charge density operators,

$$\hat{h}_j = - \sum_{j' \in \Lambda} \sum_{\alpha,\beta=1}^M t_{jj'}^{\alpha\beta} \hat{c}_{j\alpha}^\dagger \hat{c}_{j'\beta}, \quad (6)$$

and

$$\hat{n}_j = \sum_{\alpha=1}^M \hat{c}_{j\alpha}^\dagger \hat{c}_{j\alpha}, \quad (7)$$

respectively, which satisfy $\hat{H}_0 = \sum_{j \in \Lambda} \hat{h}_j$ and $\hat{N} = \sum_{j \in \Lambda} \hat{n}_j$ respectively.

We will also have reason to consider the charge-current operator, which is most simply defined as the rate of change of the center-of-charge operator $\hat{\mathbf{X}} = \sum_{j \in \Lambda} \sum_{\alpha=1}^M \mathbf{R}_{j\alpha} \hat{n}_{j\alpha}$, yielding the general expression

$$\hat{\mathbf{J}} = \frac{d}{dt} \hat{\mathbf{X}} = \int_{\text{BZ}} \frac{d\mathbf{k}}{V_{\text{BZ}}} \sum_{\alpha,\beta=1}^M \partial_{\mathbf{k}} h_{\alpha\beta}(\mathbf{k}) \hat{c}_\alpha^\dagger(\mathbf{k}) \hat{c}_\beta(\mathbf{k}). \quad (8)$$

For the examples of interest in this paper, $\hat{\mathbf{J}} = \sum_{j \in \Lambda} \hat{\mathbf{j}}_j$ is a local operator and we will verify explicitly that the current density operators $\hat{\mathbf{j}}_j$ satisfy a microscopic continuity equation that justifies the definition Eq. (8). As discussed above, Eq. (8) neglects possible off-diagonal contributions to the center-of-charge operator [43–45], but this does not affect the validity of our predictions for quantities linear in $\hat{\mathbf{j}}_j$, such as expectation values of the local current density.

B. Definition of the orbital Wigner function

We define the *orbital Wigner operator* at position \mathbf{x} and crystal momentum \mathbf{k} by

$$\hat{W}_{\alpha\beta}(\mathbf{x}, \mathbf{k}) = \int_{\text{BZ}} \frac{d\mathbf{q}}{V_{\text{BZ}}} e^{i\mathbf{q} \cdot \mathbf{x}} \hat{c}_\alpha^\dagger(\mathbf{k} - \mathbf{q}/2) \hat{c}_\beta(\mathbf{k} + \mathbf{q}/2). \quad (9)$$

The momentum and position marginals of this Wigner operator have two important properties that any single-particle Wigner operator ought to satisfy [27, 33]. First,

the momentum marginals satisfy the condition

$$\sum_{j \in \Lambda} \hat{W}_{\alpha\beta}(\mathbf{R}_{j\alpha}, \mathbf{k}) = \hat{c}_{\alpha}^{\dagger}(\mathbf{k}) \hat{c}_{\beta}(\mathbf{k}). \quad (10)$$

Second, the integral of diagonal elements of the Wigner operator over pseudomomentum \mathbf{k} at fixed $\mathbf{x} = \mathbf{R}_{j\alpha}$ is given by

$$\int_{\text{BZ}} \frac{d\mathbf{k}}{V_{\text{BZ}}} \hat{W}_{\alpha\alpha}(\mathbf{R}_{j\alpha}, \mathbf{k}) = \hat{c}_{j\alpha}^{\dagger} \hat{c}_{j\alpha}, \quad (11)$$

which is the physical charge density at the position $\mathbf{R}_{j\alpha}$. The latter property in particular means that an accurate model for the dynamics of $\hat{W}_{\alpha\beta}$ will yield correspondingly accurate predictions for the dynamics of the local charge density. Finally, a (matrix-valued) *orbital Wigner function* $w_{\alpha\beta}(\mathbf{x}, \mathbf{k})$ can be defined from the orbital Wigner operator by fixing an initial density matrix $\hat{\rho}$, and considering the expectation value

$$w_{\alpha\beta}(\mathbf{x}, \mathbf{k}) := \langle \hat{W}_{\beta\alpha}(\mathbf{x}, \mathbf{k}) \rangle, \quad (12)$$

where we use the notation $\langle \hat{O} \rangle = \text{Tr}[\hat{\rho}\hat{O}]$ for expectation values of operators \hat{O} throughout this paper. This definition can be seen as a generalization of the lattice Wigner functions discussed in Refs. [27, 29, 31–33] and the “block Wigner functions” introduced for spin-1/2 chains in Refs. [28, 30] to arbitrary crystal structures in any spatial dimension.

The reader might wonder why we are not attempting to use Bloch electrons rather than orbital electrons to construct the Wigner operator, as is standard in all Wigner-function-based treatments of Bloch electron dynamics above one spatial dimension that we are aware of (see Refs. [12–25] and references therein). The reason is that if one uses Bloch electrons rather than orbital electrons in the definition of the Wigner operator, see Eq. (9), the position marginals of the Wigner operator, see Eq. (11), cease to be local in space, and no longer have a straightforward interpretation as a physical charge density. The importance of this property for Wigner functions of lattice particles was pointed out in Refs. [27, 33]. Although it is possible to restore this property in certain Bloch-electron based approaches through a momentum-dependent shift of the position variable [14, 18], Eq. (11) circumvents such difficulties entirely.

In order to evolve orbital Wigner functions in time, we consider the Heisenberg-picture dynamics of the underlying orbital Wigner operator. For the tight-binding Hamiltonian Eq. (1), this yields

$$\partial_t \hat{W}_{\alpha\beta}(\mathbf{x}, \mathbf{k}, t) = i[\hat{H}_0, \hat{W}_{\alpha\beta}(\mathbf{x}, \mathbf{k}, t)], \quad (13)$$

which defines the time-dependent orbital Wigner function $w_{\alpha\beta}(\mathbf{x}, \mathbf{k}, t) := \langle \hat{W}_{\beta\alpha}(\mathbf{x}, \mathbf{k}, t) \rangle$.

C. Dynamics of densities of conserved charges

We now discuss how to compute the dynamics of charge densities from the exact orbital Wigner function

$w(\mathbf{x}, \mathbf{k}, t)$. By Eq. (11), it follows that the exact local charge density $n(\mathbf{R}_j, t) := \langle \hat{n}_j(t) \rangle$ at a given lattice site can be expressed as

$$n(\mathbf{R}_j, t) = \int_{\text{BZ}} \frac{d\mathbf{k}}{V_{\text{BZ}}} \text{Tr}[w(\mathbf{R}_j, \mathbf{k}, t)]. \quad (14)$$

(Note that the trace here is over internal orbital indices rather than the full Hilbert space.)

More generally, for any translation-invariant fermion bilinear $\hat{Q} = \sum_{j \in \Lambda} \hat{q}_j$ with

$$\hat{Q} = \int_{\text{BZ}} \frac{d\mathbf{k}}{V_{\text{BZ}}} \sum_{\alpha, \beta=1}^M q_{\alpha\beta}(\mathbf{k}) \hat{c}_{\alpha}^{\dagger}(\mathbf{k}) \hat{c}_{\beta}(\mathbf{k}), \quad (15)$$

the expectation value of the total charge \hat{Q} is given by

$$\langle \hat{Q}(t) \rangle = \sum_{j \in \Lambda} \int_{\text{BZ}} \frac{d\mathbf{k}}{V_{\text{BZ}}} \sum_{\alpha, \beta=1}^M q_{\alpha\beta}(\mathbf{k}) w_{\beta\alpha}(\mathbf{R}_j, \mathbf{k}, t) \quad (16)$$

by Eq. (10). However, for bilinears \hat{Q} whose densities \hat{q}_j extend over multiple sites, the global-to-local correspondence is generally less simple than suggested by Eq. (14). For example, the approximation

$$q(\mathbf{R}_j, t) \approx \int_{\text{BZ}} \frac{d\mathbf{k}}{V_{\text{BZ}}} \text{Tr}[w(\mathbf{R}_j, \mathbf{k}, t) q(\mathbf{k})] \quad (17)$$

to the exact density $q(\mathbf{R}_j, t) := \langle \hat{q}_j(t) \rangle$ generally holds only up to lattice-scale corrections. This is true for the charge-current density studied in this paper, for which Eq. (8) predicts the approximation

$$\mathbf{j}(\mathbf{R}_j, t) \approx \int_{\text{BZ}} \frac{d\mathbf{k}}{V_{\text{BZ}}} \text{Tr}[w(\mathbf{R}_j, \mathbf{k}, t) \partial_{\mathbf{k}} h(\mathbf{k}, t)] \quad (18)$$

to the exact local charge-current density $\mathbf{j}(\mathbf{R}_j, t) = \langle \hat{\mathbf{j}}_j(t) \rangle$.

It is sometimes possible to derive analogues of the exact relation in Eq. (14) (and its underlying identity in Eq. (11)) for other fermion bilinears, including the charge current. However, this must be done on a model-dependent basis. For the ballistic-scale dynamics and observables of interest in this paper, the lattice-scale corrections to Eq. (17) are negligibly small and can safely be ignored.

D. Derivation of ballistic-scale transport equation

We now summarize the derivation of a ballistic-scale transport equation from the exact Heisenberg equation of motion Eq. (13), following recent derivations of the Boltzmann equation for lattice Wigner functions in one spatial dimension [28, 32, 33]. To derive a transport equation for $w_{\alpha\beta}$, note that the Heisenberg-picture evolution

of momentum-space fermions is given by $i[\hat{H}_0, \hat{c}_\alpha(\mathbf{k}, t)] = -i \sum_{\gamma=1}^M h_{\alpha\gamma}(\mathbf{k}) \hat{c}_\gamma(\mathbf{k}, t)$, which yields

$$\begin{aligned} \partial_t \hat{W}_{\alpha\beta}(\mathbf{x}, \mathbf{k}, t) &= i \sum_{\gamma=1}^M \int_{BZ} \frac{d\mathbf{q}}{V_{BZ}} e^{i\mathbf{q}\cdot\mathbf{x}} \\ &\left(h_{\gamma\alpha}(\mathbf{k} - \mathbf{q}/2) \hat{c}_\gamma^\dagger(\mathbf{k} - \mathbf{q}/2) c_\beta(\mathbf{k} + \mathbf{q}/2) \right. \\ &\left. - h_{\beta\gamma}(\mathbf{k} + \mathbf{q}/2) \hat{c}_\alpha^\dagger(\mathbf{k} - \mathbf{q}/2) c_\gamma(\mathbf{k} + \mathbf{q}/2) \right), \quad (19) \end{aligned}$$

where we used Hermiticity of the Bloch Hamiltonian $h_{\alpha\beta}(\mathbf{k})^* = h_{\beta\alpha}(\mathbf{k})$. Using the definition of the Wigner operator to close this system of equations then yields

$$\begin{aligned} \partial_t \hat{W}_{\alpha\beta}(\mathbf{x}, \mathbf{k}, t) &= -i \sum_{\gamma=1}^M \sum_{\mathbf{r} \in \Lambda} \left(t^{\gamma\alpha}(\mathbf{r}) e^{-i\mathbf{k}\cdot\mathbf{r}\tau_\alpha} \hat{W}_{\gamma\beta}(\mathbf{x} + \mathbf{r}_{\gamma\alpha}/2, \mathbf{k}, t) \right. \\ &\left. - t^{\beta\gamma}(\mathbf{r}) e^{-i\mathbf{k}\cdot\mathbf{r}\tau_\beta} \hat{W}_{\alpha\gamma}(\mathbf{x} - \mathbf{r}_{\beta\gamma}/2, \mathbf{k}, t) \right), \quad (20) \end{aligned}$$

where $\mathbf{r}_{\alpha\beta} := \mathbf{r} + \boldsymbol{\tau}_\alpha - \boldsymbol{\tau}_\beta$ denote relative spatial positions within the crystal lattice.

So far, our analysis has been exact. We now Taylor expand about \mathbf{x} to yield a derivative expansion in the spatial gradient $\partial_{\mathbf{x}}$. A full discussion, including higher-order corrections in $\partial_{\mathbf{x}}$, is given in Appendix B. Interestingly, this expansion shows that the inclusion of quantum coherence cannot generically change the ballistic nature of transport in finite-range, non-interacting systems. In this paper, we therefore focus on the ballistic or Euler scaling limit [42] as $\|\mathbf{x}\|, t \rightarrow \infty$. This is precisely the regime of validity of the usual free-streaming Boltzmann equation. In this limit, terms of order $\mathcal{O}(\partial_{\mathbf{x}}^2)$ in spatial derivatives can be neglected, and taking expectation values of the operator equations of motion with respect to the initial density matrix yields the transport equation

$$\begin{aligned} \partial_t w(\mathbf{x}, \mathbf{k}, t) &= -i [h(\mathbf{k}), w(\mathbf{x}, \mathbf{k}, t)] \\ &- \frac{1}{2} \sum_{a=1}^d \{ \partial_{k_a} h(\mathbf{k}), \partial_{x_a} w(\mathbf{x}, \mathbf{k}, t) \}. \quad (21) \end{aligned}$$

for the matrix-valued orbital Wigner function w .

Substituting the approximate Wigner function $w(\mathbf{x}, \mathbf{k}, t)$ resulting from solving Eq. (21) into Eqs. (14) and (18) yields ballistic-scale transport-theory predictions for the exact quantities $n(\mathbf{R}_j, t)$ and $\mathbf{j}(\mathbf{R}_j, t)$, which we denote by $n_{\text{Wigner}}(\mathbf{x}, t)$ and $\mathbf{j}_{\text{Wigner}}(\mathbf{x}, t)$ respectively. Given that the only approximation involved in deriving these expressions from Eq. (1) lies in the neglect of lattice-scale corrections, we expect these predictions to become exact in the ballistic scaling limit, as for the ordinary free-streaming Boltzmann equation.

E. Initial conditions

For any initial density matrix $\hat{\rho}$, the exact initial condition for the Wigner function $w_{\alpha\beta}$ is given in principle by Eq. (12). However, this expression can be cumbersome to evaluate in practice and it will be useful to instead introduce approximate but easy-to-calculate initial conditions for $w_{\alpha\beta}$ that model the ‘‘local equilibrium states’’ of interest in transport theory. Recall that slowly varying initial temperature and chemical potential profiles $\beta(\mathbf{x})$ and $\mu(\mathbf{x})$ define local equilibrium states of the form

$$\hat{\rho} \propto \exp \left(- \sum_{j \in \Lambda} \beta(\mathbf{R}_j) [\hat{h}_j - \mu(\mathbf{R}_j) \hat{n}_j] \right), \quad (22)$$

where \hat{h}_j and \hat{n}_j denote the energy and charge density operators defined in Eqs. (6) and (7) respectively. In order to model these, let us first consider the Wigner function for initial states in *global* thermal equilibrium, $\hat{\rho} \propto e^{-\beta(\hat{H}_0 - \mu \hat{N})}$. In terms of the changes of basis to Bloch electrons $U(\mathbf{k})$ defined in Eq. (4), the exact result

$$w_{\alpha\beta}(\mathbf{k}) = \sum_{n=1}^M U_{\alpha n}(\mathbf{k}) \frac{1}{1 + e^{\beta(E_n(\mathbf{k}) - \mu)}} U_{n\beta}^\dagger(\mathbf{k}), \quad (23)$$

follows by Fermi-Dirac statistics. By definition of $U(\mathbf{k})$, this can be written in matrix form in terms of the Bloch Hamiltonian $h(\mathbf{k})$ as

$$w(\mathbf{k}) = \frac{1}{1 + e^{\beta(h(\mathbf{k}) - \mu)}}. \quad (24)$$

In the local density approximation (whose rigorous justification requires substantial effort [46] and will not be pursued here) and in the same notation, the initial condition corresponding to Eq. (22) can be written as

$$w(\mathbf{x}, \mathbf{k}, 0) = \frac{1}{1 + e^{\beta(\mathbf{x})(h(\mathbf{k}) - \mu(\mathbf{x}))}}, \quad (25)$$

which is expected to be accurate whenever the length scale of variation of $\beta(\mathbf{x})$ and $\mu(\mathbf{x})$ is much larger than the typical correlation length of the state in Eq. (22). More precisely, we expect that provided $\max_{\mathbf{x}} \beta(\mathbf{x}) < \infty$, Eq. (25) can be made to hold to an arbitrarily good approximation by taking the scale of variation of $\beta(\mathbf{x})$ and $\mu(\mathbf{x})$ to be sufficiently large. We will use this expression for comparison with microscopic numerical simulations of time evolution from Eq. (22) below.

We will also be interested in more strongly non-equilibrium initial conditions that consist of preparing a local equilibrium state (22) and then applying an inhomogeneous and slowly varying phase texture $\varphi_\alpha(\mathbf{x})$ in real space, $\hat{c}_{j\alpha} \mapsto e^{-i\varphi_\alpha(\mathbf{R}_{j\alpha})} \hat{c}_{j\alpha}$. Such initial states can in principle be prepared and measured using present-day experimental capabilities [47–50]. Let us write

$$\hat{h}'_j = - \sum_{j' \in \Lambda} \sum_{\alpha, \beta=1}^M t_{jj'}^{\alpha\beta} e^{i(\varphi_\alpha(\mathbf{R}_{j\alpha}) - \varphi_\beta(\mathbf{R}_{j'\beta}))} \hat{c}_{j\alpha}^\dagger \hat{c}_{j'\beta} \quad (26)$$

for the modified local Hamiltonian under this mapping. Then the initial condition in question is given explicitly by

$$\hat{\rho}' \propto \exp \left(- \sum_{j \in \Lambda} \beta(\mathbf{R}_j) [\hat{h}'_j - \mu(\mathbf{R}_j) \hat{n}_j] \right). \quad (27)$$

In the local density approximation, the initial Wigner function (25) modeling Eq. (27) is modified to

$$w_{\alpha\beta}(\mathbf{x}, \mathbf{k}, 0) \mapsto e^{i[\varphi_\alpha(\mathbf{x}) - \varphi_\beta(\mathbf{x})]} w_{\alpha\beta}(\mathbf{x}, \mathbf{k}, 0) \quad (28)$$

at leading order in spatial derivatives $\partial_{\mathbf{x}}\varphi_\alpha$. A nontrivial probe of such initial phase coherence is the two-point correlation function $\hat{c}_{j\alpha}^\dagger \hat{c}_{j\beta}$ between two basis sites within the same unit cell. We can extract this information from the Wigner function using the identity

$$\int_{\text{BZ}} \frac{d\mathbf{k}}{V_{\text{BZ}}} e^{-i\mathbf{k} \cdot (\boldsymbol{\tau}_\alpha - \boldsymbol{\tau}_\beta)} w_{\beta\alpha}(\mathbf{R}_j + (\boldsymbol{\tau}_\alpha + \boldsymbol{\tau}_\beta)/2, \mathbf{k}) = \langle \hat{c}_{j\alpha}^\dagger \hat{c}_{j\beta} \rangle. \quad (29)$$

F. Time-dependent Hamiltonians

We now consider allowing the tight-binding Hamiltonian Eq. (1) to depend on time via its hopping amplitudes $t_{\alpha\beta}(\mathbf{r}, t)$. Such an extension of our formalism is necessary to capture topological effects such as Thouless pumping [34]. In Fourier space, this yields the time-dependent Hamiltonian

$$\hat{H}_0(t) = \int_{\text{BZ}} \frac{d\mathbf{k}}{V_{\text{BZ}}} \sum_{\alpha, \beta=1}^M h_{\alpha\beta}(\mathbf{k}, t) \hat{c}_\alpha^\dagger(\mathbf{k}) \hat{c}_\beta(\mathbf{k}), \quad (30)$$

where the time-dependent Bloch Hamiltonian

$$h_{\alpha\beta}(\mathbf{k}, t) = - \sum_{j \in \Lambda} t_{\alpha\beta}(\mathbf{R}_j, t) e^{-i\mathbf{k} \cdot (\mathbf{R}_j + \boldsymbol{\tau}_\alpha - \boldsymbol{\tau}_\beta)}. \quad (31)$$

The change of basis to Bloch electrons now depends on time, i.e. for each \mathbf{k} , there exist $U(\mathbf{k}, t)$ such that

$$\sum_{\alpha, \beta=1}^M U_{m\alpha}^\dagger(\mathbf{k}, t) h_{\alpha\beta}(\mathbf{k}, t) U_{\beta n}(\mathbf{k}, t) = E_n(\mathbf{k}, t) \delta_{mn}. \quad (32)$$

which defines M time-dependent energy bands $\{E_n(\mathbf{k}, t)\}_{n=1}^M$ and time-dependent Bloch electron creation operators

$$\hat{d}_n^\dagger(\mathbf{k}, t) = \sum_{\alpha=1}^M U_{\alpha n}(\mathbf{k}, t) \hat{c}_\alpha^\dagger(\mathbf{k}), \quad (33)$$

in terms of which

$$\hat{H}_0(t) = \int_{\text{BZ}} \frac{d\mathbf{k}}{V_{\text{BZ}}} \sum_{n=1}^M E_n(\mathbf{k}, t) \hat{d}_n^\dagger(\mathbf{k}, t) \hat{d}_n(\mathbf{k}, t). \quad (34)$$

A special case that admits further simplification is periodic-in-time or Floquet dynamics $\hat{H}_0(t+T) = \hat{H}_0(t)$, see Refs. [51, 52] for proposed ‘‘Floquet-Boltzmann’’ equations that capture such dynamics. (However, these works focus on diagonal elements of the Wigner function in the basis of Bloch electrons, which is distinct from the approach pursued here.) Such simplifications arising from periodicity in time will not be necessary for our purposes and our transport equation instead allows for arbitrary time dependence, which both encompasses the time-independent case discussed above and matches microscopic numerical simulations in the time-periodic case (see Section IV).

By repeating the derivation of Eq. (21) in the time-dependent setting, we obtain the ballistic-scale transport equation

$$\partial_t w(\mathbf{x}, \mathbf{k}, t) = -i[h(\mathbf{k}, t), w(\mathbf{x}, \mathbf{k}, t)] - \frac{1}{2} \sum_{a=1}^d \{ \partial_{k_a} h(\mathbf{k}, t), \partial_{x_a} w(\mathbf{x}, \mathbf{k}, t) \}. \quad (35)$$

G. External electric fields and Bloch oscillations

An important feature of any transport theory is its ability to make predictions in the presence of external electric and magnetic fields. Since this paper is dedicated to the nontrivial quantum effects that arise even in the absence of such fields, we will largely defer a detailed discussion of electric fields (and all discussion of magnetic fields) to future work.

However, for completeness we derive a ballistic-scale equation of motion in the presence of an external electrostatic potential

$$\hat{V} = \sum_{j \in \Lambda} \sum_{\alpha=1}^M V(\mathbf{R}_{j\alpha}) \hat{c}_{j\alpha}^\dagger \hat{c}_{j\alpha}, \quad (36)$$

so that the total Hamiltonian becomes

$$\hat{H} = \hat{H}_0 + \hat{V}. \quad (37)$$

(Note that we have neglected off-diagonal contributions to \hat{V} [43–45], which limits our accuracy to linear order in applied electric fields. However, such corrections could in principle be included in our approach and would modify Eq. (39) accordingly.) In position space and letting $\bar{\mathbf{R}}_{jj'}^{\alpha\beta} = (\mathbf{R}_{j\alpha} + \mathbf{R}_{j'\beta})/2$, the orbital Wigner operator can be expressed in terms of the Brillouin delta function $\delta_B(\mathbf{x})$ (see Appendix A) as

$$\hat{W}_{\alpha\beta}(\mathbf{x}, \mathbf{k}) = \sum_{j, j' \in \Lambda} \delta_B(\mathbf{x} - \bar{\mathbf{R}}_{jj'}^{\alpha\beta}) e^{i\mathbf{k} \cdot (\mathbf{R}_{j\alpha} - \mathbf{R}_{j'\beta})} \hat{c}_{j\alpha}^\dagger \hat{c}_{j'\beta}. \quad (38)$$

By manipulating this expression (see Appendix C), we

obtain the ballistic-scale transport equation

$$\begin{aligned} \partial_t w(\mathbf{x}, \mathbf{k}, t) &= -i[h(\mathbf{k}), w(\mathbf{x}, \mathbf{k}, t)] \\ &\quad - \frac{1}{2} \sum_{a=1}^d \{ \partial_{k_a} h(\mathbf{k}), \partial_{x_a} w(\mathbf{x}, \mathbf{k}, t) \} \\ &\quad - e \partial_{\mathbf{x}} \phi(\mathbf{x}) \cdot \partial_{\mathbf{k}} w(\mathbf{x}, \mathbf{k}, t) \end{aligned} \quad (39)$$

in the presence of an external electrostatic potential $V(\mathbf{x}) = -e\phi(\mathbf{x})$. For a single band for which the Wigner and Boltzmann formalisms coincide, this recovers the standard Boltzmann forcing term [8] as expected. Using this method, one can in principle compute higher-order corrections to the transport equation in momentum derivatives of w but the lack of spatial localization of the Brillouin delta function $\delta_{\mathbf{B}}(\mathbf{x})$ means that the resulting expressions are not very illuminating. We note that Eq. (39) generalizes straightforwardly to time-dependent Hamiltonians and potentials, provided the latter are accompanied by negligible magnetic fields.

In the special case of a spatially uniform electrostatic field $\phi(\mathbf{x}) = -\mathbf{E} \cdot \mathbf{x}$, such higher-order corrections in $\partial_{\mathbf{k}}$ vanish and Eq. (39) admits a simplification analogous to the emergence of Bloch oscillations in ordinary semiclassical transport theory. To see this, suppose that the electrostatic field is uniform and define the accelerating-frame Wigner function $u(\mathbf{x}, \mathbf{k}, t)$ via the relation

$$w(\mathbf{x}, \mathbf{k}, t) = u(\mathbf{x}, \mathbf{k} + e\mathbf{E}t, t) \quad (40)$$

at each time t . Then u satisfies the force-free but time-dependent system of partial differential equations

$$\begin{aligned} \partial_t u(\mathbf{x}, \mathbf{k}, t) &= -i[h(\mathbf{k} - e\mathbf{E}t), u(\mathbf{x}, \mathbf{k}, t)] \\ &\quad - \frac{1}{2} \sum_{a=1}^d \{ \partial_{k_a} h(\mathbf{k} - e\mathbf{E}t), \partial_{x_a} u(\mathbf{x}, \mathbf{k}, t) \}, \end{aligned} \quad (41)$$

which is a special case of Eq. (35). Thus, just as in the usual semiclassical theory of Bloch oscillations [8], it is always possible to eliminate a uniform, time-independent electrostatic field in Eq. (39) by passing to a uniformly accelerating frame of reference, at the price of making the effective Bloch Hamiltonian time-dependent. In fact this conclusion holds at higher orders in spatial derivatives too (see Appendix C).

H. Methods of solution

1. General considerations

The transport equation (21) and its time-dependent generalization Eq. (35) are linear, first-order PDEs and therefore always amenable to a numerical solution based on finite-difference methods [53] or Fourier analysis. We pursue both approaches in this work and two possible numerical schemes are summarized in Appendix D.

A striking and immediate property of these equations, shared by other Wigner-function based equations of motion [14–25], is that they exhibit M^2 propagation velocities at any given instant of time, rather than the M quasiparticle group velocities $\{\partial_{\mathbf{k}} E_n(\mathbf{k})\}_{n=1}^M$ within each band that determine ordinary semiclassical transport. We will explore this observation in more detail below.

For now, we merely note that the smaller the number of bands M , the more tractable Eq. (21) becomes. The simplest cases are $M = 1$ (a single band), for which the orbital Wigner function recovers conventional Boltzmann theory at leading order in spatial derivatives [28, 32], and $M = 2$ bands, which is the simplest case that exhibits effects beyond Boltzmann theory and will be the main focus of this paper.

For the two-band systems considered in this paper, we obtain predictions for orbital Wigner function dynamics by solving Eq. (21) numerically on a sufficiently dense grid of k -points in the Brillouin zone, using a second-order staggered leapfrog method [53] for Figs. 1–5 and a more efficient GPU-based Fourier-kernel method for the most numerically demanding Fig. 6, see Appendix D for further details.

2. Solvable special case: vanishing Berry connection

In general, we expect that the non-trivial \mathbf{k} -dependence of the Bloch eigenvectors (i.e. of the matrix $U(\mathbf{k})$ defined in Eq. (4)) precludes a simple exact solution to Eq. (21). In the special case that $U(\mathbf{k})$ is differentiable in \mathbf{k} and defines a vanishing Berry connection $\mathcal{A}_a(\mathbf{k}) = -iU(\mathbf{k})^\dagger \partial_{k_a} U(\mathbf{k}) = 0$, such a solution is possible. Since its derivation is instructive, and because it may be found useful for benchmarking numerical approaches, we now summarize this closed-form solution.

First define the *band Wigner function*

$$\tilde{w}(\mathbf{x}, \mathbf{k}, t) = U^\dagger(\mathbf{k}) w(\mathbf{x}, \mathbf{k}, t) U(\mathbf{k}), \quad (42)$$

(this is analogous to the “decoupling” step in Refs. [17, 18]) and the diagonalized Bloch Hamiltonian $\tilde{h}(\mathbf{k}) = U^\dagger(\mathbf{k}) h(\mathbf{k}) U(\mathbf{k})$ as in Eq. (4). Then, substituting into Eq. (21) and suppressing arguments, we find that

$$\partial_t \tilde{w} + \frac{1}{2} \sum_{a=1}^d \{ U^\dagger(\partial_{k_a} h) U, \partial_{x_a} \tilde{w} \} = -i[\tilde{h}, \tilde{w}]. \quad (43)$$

To simplify the streaming term, note that by differentiability of $U(\mathbf{k})$, $\partial_{k_a} U(\mathbf{k}) = -U^\dagger(\mathbf{k}) (\partial_{k_a} U(\mathbf{k})) U^\dagger(\mathbf{k})$ and therefore

$$U^\dagger(\mathbf{k}) (\partial_{k_a} h(\mathbf{k})) U(\mathbf{k}) = \partial_{k_a} \tilde{h}(\mathbf{k}) + i[\mathcal{A}_a(\mathbf{k}), \tilde{h}(\mathbf{k})], \quad (44)$$

where we defined the Berry connection through its components $\mathcal{A}_a(\mathbf{k}) = -iU^\dagger(\mathbf{k}) \partial_{k_a} U(\mathbf{k})$. Restoring matrix

indices, it follows that

$$\begin{aligned} \partial_t \tilde{w}_{mn} + \frac{1}{2} \sum_{a=1}^d \left(\{ \partial_{k_a} \tilde{h} + i[\mathcal{A}_a, \tilde{h}], \partial_{x_a} \tilde{w} \} \right)_{mn} \\ = -i(E_m - E_n) \tilde{w}_{mn}. \end{aligned} \quad (45)$$

Although this equation is always exactly solvable by linearity, the resulting solution does not appear to be especially tractable in general. An exception is the special case $\mathcal{A}_a(\mathbf{k}) = 0$ for all \mathbf{k} , in which Eq. (45) reduces to

$$\partial_t \tilde{w}_{mn} + \bar{\mathbf{v}}_{mn} \cdot \partial_{\mathbf{x}} \tilde{w}_{mn} = -i E_{mn} \tilde{w}_{mn}, \quad (46)$$

where we defined $E_{mn}(\mathbf{k}) := E_m(\mathbf{k}) - E_n(\mathbf{k})$ and a “mean group velocity” $\bar{\mathbf{v}}_{mn}(\mathbf{k}) = \frac{1}{2} \partial_{\mathbf{k}} (E_m(\mathbf{k}) + E_n(\mathbf{k}))$. Eq. (46) is now simple enough to be solved in closed form, and the solution to its initial value problem reads

$$\tilde{w}_{mn}(\mathbf{x}, \mathbf{k}, t) = e^{-i E_{mn}(\mathbf{k}) t} \tilde{w}_{mn}(\mathbf{x} - \bar{\mathbf{v}}_{mn}(\mathbf{k}) t, \mathbf{k}, 0). \quad (47)$$

In terms of the orbital Wigner function, the resulting solution to Eq. (21) is given by

$$\begin{aligned} w_{\alpha\beta}(\mathbf{x}, \mathbf{k}, t) &= \sum_{\alpha', \beta', m, n=1}^M e^{-i E_{mn}(\mathbf{k}) t} U_{\alpha m}(\mathbf{k}) U_{m\alpha'}^\dagger(\mathbf{k}) \\ &w_{\alpha'\beta'}(\mathbf{x} - \bar{\mathbf{v}}_{mn}(\mathbf{k}) t, \mathbf{k}, 0) U_{\beta'n}(\mathbf{k}) U_{n\beta}^\dagger(\mathbf{k}). \end{aligned} \quad (48)$$

III. COMPARISON TO SEMICLASSICAL TRANSPORT THEORY

We now test the validity of the orbital Wigner function approach, compared to conventional semiclassical transport theory, against numerically exact free-fermion simulations. We first consider states that are locally in thermal equilibrium at a non-zero temperature, for which we do not expect any deviations from textbook results [8]. We present a general analytical argument for how orbital Wigner functions recover semiclassical transport theory in local thermal equilibrium, before illustrating this point through a free-fermion simulation of charge and current dynamics in a two-band example.

We next consider initial states with spatially-inhomogeneous single-particle quantum coherence, which lie beyond the scope of semiclassical transport theory. We specifically focus on quantum coherence between orbitals within each unit cell, as might be prepared in an ultracold atom device [47–49] or through scanning tunneling microscopy of a material sample [50]. We present numerical evidence that orbital Wigner functions are well-suited for capturing relaxation from such quantum-coherent initial states.

A. Essentials of semiclassical transport theory

For generic choices of hoppings, we may assume that the energy bands do not intersect, $E_1(\mathbf{k}) > E_2(\mathbf{k}) \dots >$

$E_M(\mathbf{k})$ (note that this assumption is not needed for our orbital Wigner function formalism, but rather to facilitate comparison with conventional transport theory). Then, defining group velocities $\mathbf{v}_n(\mathbf{k}) = \partial_{\mathbf{k}} E_n(\mathbf{k})$, conventional semiclassical transport theory in the absence of interactions and external fields describes the time evolution of the “local density of occupied states” $\rho_n(\mathbf{x}, \mathbf{k}, t)$ of the n th band via the Boltzmann equation [8]

$$\partial_t \rho_n + \mathbf{v}_n(\mathbf{k}) \cdot \partial_{\mathbf{x}} \rho_n = 0, \quad (49)$$

with solution

$$\rho_n(\mathbf{x}, \mathbf{k}, t) = \rho_n(\mathbf{x} - \mathbf{v}_n(\mathbf{k}) t, \mathbf{k}, 0). \quad (50)$$

In thermal equilibrium states, $\hat{\rho} \propto e^{-\beta(\hat{H}_0 - \mu \hat{N})}$, we have

$$\rho_n(\mathbf{k}) = \frac{1}{1 + e^{\beta(E_n(\mathbf{k}) - \mu)}}, \quad (51)$$

which in the local density approximation yields the initial condition

$$\rho_n(\mathbf{x}, \mathbf{k}, 0) = \frac{1}{1 + e^{\beta(\mathbf{x})(E_n(\mathbf{k}) - \mu(\mathbf{x}))}} \quad (52)$$

for locally thermal initial states in Eq. (22). Predictions for the dynamics of local observables such as the charge density $n(\mathbf{x}, t)$ and charge-current density $\mathbf{j}(\mathbf{x}, t)$ are then given by

$$n_{\text{Boltzmann}}(\mathbf{x}, t) = \int_{\text{BZ}} \frac{d\mathbf{k}}{V_{\text{BZ}}} \sum_{n=1}^M \rho_n(\mathbf{x}, \mathbf{k}, t) \quad (53)$$

and

$$\mathbf{j}_{\text{Boltzmann}}(\mathbf{x}, t) = \int_{\text{BZ}} \frac{d\mathbf{k}}{V_{\text{BZ}}} \sum_{n=1}^M \rho_n(\mathbf{x}, \mathbf{k}, t) \mathbf{v}_n(\mathbf{k}) \quad (54)$$

respectively.

B. Dynamics of local equilibrium states

We commented earlier that the equations of motion for the orbital Wigner function Eq. (21) were characterized by M^2 propagation velocities, rather than the M quasiparticle group velocities that appear in the semiclassical theory. On the other hand, we expect the semiclassical theory to yield accurate results near thermal equilibrium, for example for time evolution from local equilibrium initial states of the form in Eq. (22).

In fact there is no contradiction between these claims, and in hydrodynamic regimes for which the system is locally near thermal equilibrium, the orbital Wigner dynamics closely approximates Boltzmann dynamics and is dominated by M “diagonal” degrees of freedom that propagate at the quasiparticle group velocity. In this section, we first verify analytically that this claim holds instantaneously for locally equilibrated Wigner functions

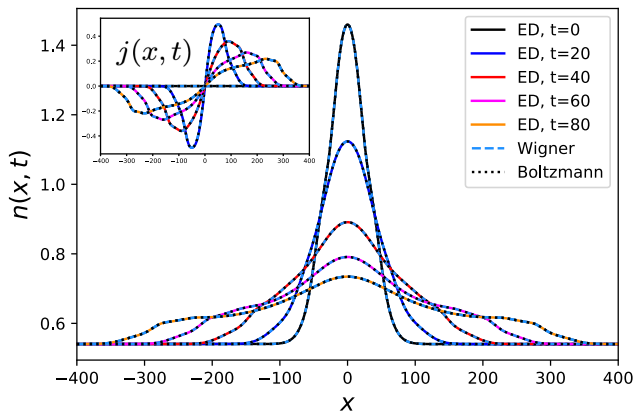


FIG. 1. **Main figure:** Time evolution from a localized initial charge density under the Hamiltonian (58), with uniform initial temperature $\beta = 1$ and initial chemical potential profile as in Eq. (61), with bulk chemical potential $\mu_0 = -4$, central chemical potential $\mu_1 = 4$ and length scale $l = 40$ sites. The agreement between microscopic exact diagonalization (solid lines), Wigner function predictions (light blue dashed lines) and Boltzmann equation predictions (black dotted lines) is clear. **Inset:** Predictions for the charge-current density $j(x, t)$ versus numerics.

of the form in Eq. (25). We then check numerically that the time evolution of charge density from local equilibrium initial conditions (22) is accurately captured by the Wigner-function transport equation (21) in a two-band example.

For the analytical argument, we take as our starting point the transport equation (45) for the band Wigner function. For an orbital Wigner function that is instantaneously in local equilibrium, so that

$$w(\mathbf{x}, \mathbf{k}, t) = \frac{1}{1 + e^{\beta(\mathbf{x}, t)(h(\mathbf{k}) - \mu(\mathbf{x}, t))}}, \quad (55)$$

the band Wigner function is diagonal,

$$\tilde{w}_{mn}(\mathbf{x}, \mathbf{k}, t) = \frac{\delta_{mn}}{1 + e^{\beta(\mathbf{x}, t)(E_n(\mathbf{k}) - \mu(\mathbf{x}, t))}}. \quad (56)$$

Thus the off-diagonal components of Eq. (45) can be ignored in the vicinity of time t , leaving the evolution equation

$$\partial_t \tilde{w}_{nn} + \frac{1}{2} \sum_{a=1}^d \left(\{ \partial_{k_a} \tilde{h} + i[\mathcal{A}_a, \tilde{h}], \partial_{x_a} \tilde{w} \} \right)_{nn} = 0$$

for the diagonal components. Evaluating the anticommutator directly and using the fact that \tilde{h} is diagonal then yields

$$\partial_t \tilde{w}_{nn}(\mathbf{x}, \mathbf{k}, t) + \mathbf{v}_n(\mathbf{k}) \cdot \partial_{\mathbf{x}} \tilde{w}_{nn}(\mathbf{x}, \mathbf{k}, t) = 0. \quad (57)$$

Note that this perfectly recovers the standard Boltzmann description of time evolution from local equilibrium, provided we make the identification $\tilde{w}_{nn}(\mathbf{x}, \mathbf{k}, t) \leftrightarrow \rho_n(\mathbf{x}, \mathbf{k}, t)$.

In practice, the local equilibrium ansatz in Eq. (55) is not preserved exactly under the orbital Wigner function dynamics, and for a more stringent test, we now compare predictions from solving Eq. (21) with initial condition (25) to microscopic numerical simulations from locally thermal initial conditions in Eq. (22) in a specific two-band model.

For our numerical comparison, we choose the one-dimensional two-band Hamiltonian

$$\hat{H}_0 = \sum_{j=-L/2}^{L/2-1} (4 \hat{c}_{j,A}^\dagger \hat{c}_{j,B} - 3 \hat{c}_{j+1,A}^\dagger \hat{c}_{j,A} + \text{h.c.}). \quad (58)$$

This has Bloch Hamiltonian

$$h(k) = \begin{pmatrix} -6 \cos k & 4 \\ 4 & 0 \end{pmatrix}. \quad (59)$$

The band structure is given by $E_{\pm}(k) = -3 \cos k \pm \sqrt{16 + 9 \cos^2 k}$ and the Bloch eigenvectors are supported on both sites A and B and depend non-trivially on k . For mathematical convenience, we set the basis positions $\boldsymbol{\tau}_A = \boldsymbol{\tau}_B = 0$ within each unit cell and index the lattice sites by integers, $x_j = j$ with $-L/2 \leq x_j \leq L/2$ and periodic boundary conditions $x_{-L/2} \equiv x_{L/2}$.

For this model, the Heisenberg-picture charge density operator $\hat{n}_j = \hat{c}_{j,A}^\dagger \hat{c}_{j,A} + \hat{c}_{j,B}^\dagger \hat{c}_{j,B}$ satisfies the microscopic continuity equation

$$\partial_t \hat{n}_j + \hat{j}_{j+1} - \hat{j}_j = 0, \quad (60)$$

where the charge-current density operator $\hat{j}_j = 3i(\hat{c}_{j,A}^\dagger \hat{c}_{j-1,A} - \hat{c}_{j-1,A}^\dagger \hat{c}_{j,A})$ yields a global current operator $\hat{J} = \sum_{j=-L/2}^{L/2-1} \hat{j}_j$ that satisfies Eq. (8) in the thermodynamic limit.

We consider initializing this model in a local equilibrium state as in Eq. (22), at a uniform temperature $\beta = 1$ but with a strongly inhomogeneous chemical potential that creates a localized distribution of charge

$$\mu(x) = \mu_0 + (\mu_1 - \mu_0) e^{-x^2/l^2} \quad (61)$$

about $x = 0$, where the bulk chemical potential $\mu_0 = -4$ sits in the lower band and the central chemical potential $\mu_1 = 4$ sits in the upper band, and the length scale $l = 40$. Note that although this state is locally in thermal equilibrium, it is far from the linear response regime and thus represents a stringent test of the theory.

We perform numerically exact microscopic simulations using standard free-fermion methods [54, 55] on $L = 800$ sites, and compare the resulting dynamics of the charge density and charge-current density to Boltzmann-equation predictions in Eqs. (53) and (54) and to the Wigner-function predictions in Eq. (14) and (18) obtained by solving Eq. (21) numerically. Results are shown in the right panel of Fig. 1 and the charge and current profiles arising from these three distinct methods are indistinguishable from one another as expected.

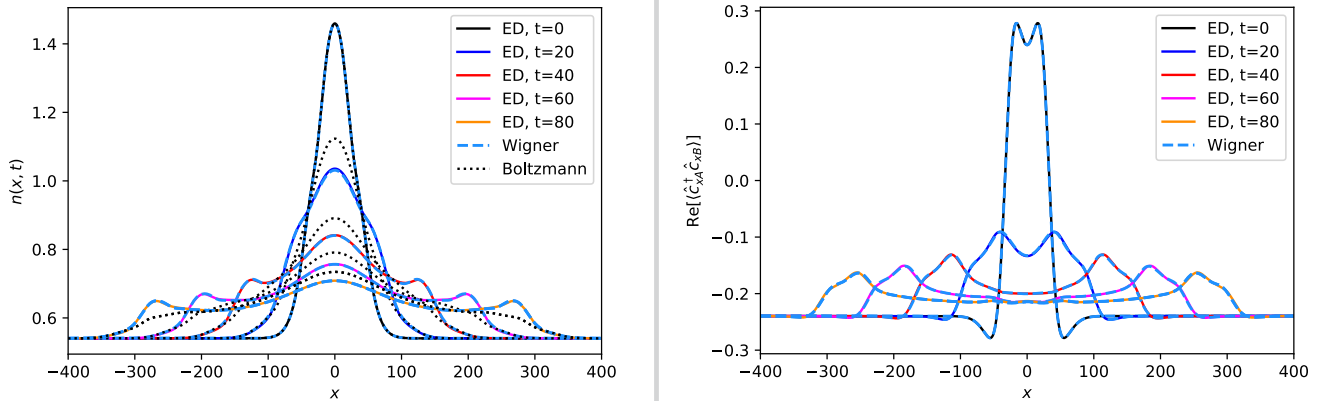


FIG. 2. **Left:** Time evolution of charge density from the initial condition in Eq. (61) with the same parameters as in Fig. 1, augmented by an inhomogeneous initial phase as in Eq. (63) with maximum relative phase $\phi = \pi$. Boltzmann theory predictions that do not account for this inhomogeneous phase (as plotted in Fig. 1) appear as black dotted lines for reference. **Right:** Wigner function predictions for the dynamics of onsite inter-orbital correlation functions. Such correlation functions are beyond conventional semiclassical transport theory and we observe excellent agreement with Wigner function predictions.

C. Phase coherence beyond semiclassical transport

We next test the orbital Wigner function approach for phase-coherent initial conditions of the form in Eq. (27). Textbook semiclassical transport theory does not make any predictions for such dynamics [8] because the initial state (27) is not even locally in thermal equilibrium with respect to \hat{H}_0 . Note however that this state *is* in local equilibrium with respect to the effective Hamiltonian $\hat{H}'_0 = \sum_{j \in \Lambda} h'_j$ with h'_j defined as in Eq. (26). (In this sense, Eq. (27) defines a kind of quantum quench [56].)

In this setting, our transport equation (21) makes predictions both for the dynamics of the local charge density $n(x, t)$ and for the dynamics of local off-diagonal correlation functions $\langle \hat{c}_{j\alpha}^\dagger \hat{c}_{j\beta} \rangle(t) = \text{Tr}[\hat{\rho}(t) \hat{c}_{j\alpha}^\dagger \hat{c}_{j\beta}]$ via Eq. (29), which here yields the prediction

$$\langle \hat{c}_{j\alpha}^\dagger \hat{c}_{j\beta} \rangle_{\text{Wigner}}(t) = \int_{\text{BZ}} \frac{dk}{V_{\text{BZ}}} w_{\beta\alpha}(x_j, k, t). \quad (62)$$

We test this prediction for the Hamiltonian in Eq. (58) considered in the previous section, with the same initial conditions consisting of a localized spot of charge as in Eq. (61), but now augment these by a relative phase with maximal value ϕ that varies spatially on the same length scale as the charge density, i.e.,

$$\varphi_A(x) = (\phi/2)e^{-x^2/l^2}, \quad \varphi_B(x) = -(\phi/2)e^{-x^2/l^2}, \quad (63)$$

giving rise to a strongly non-equilibrium initial density matrix $\hat{\rho}'$ as defined in Eq. (27).

For such initial conditions, we find excellent agreement with orbital Wigner function predictions for both $n(x, t)$ and for the onsite correlation functions $\langle \hat{c}_{j\alpha}^\dagger \hat{c}_{j\beta} \rangle(t)$, see Fig. 2 for a comparison with microscopic simulations with $\phi = \pi$. Note that the inhomogeneous initial phase in

Eq. (63) does not alter the initial charge-density profile but it does alter the initial energy density with respect to the Hamiltonian \hat{H}_0 . This is one way to understand the deviation in the left panel of Fig. 2 from Boltzmann-equation predictions for the charge dynamics that do not take the inhomogeneous initial phase in Eq. (63) into account.

IV. APPLICATION TO TIME-DEPENDENT HAMILTONIANS

Coherent driving of quantum Hamiltonians is well-known to induce coherent superpositions of quantum states; the canonical example is Rabi oscillations in two-level systems. It is therefore natural to expect that quantum coherence plays an essential role in the dynamics and transport of time-dependent multiband systems. Indeed, the adiabatic Thouless pumping of a topologically quantized unit of charge per cycle in one-dimensional insulators can be seen as a consequence of the states within a topological band accumulating a coherent global phase [34].

In this section, we perform a precision verification of the accuracy of our orbital Wigner formalism for time-dependent Hamiltonians against microscopic free-fermion simulations, which to the best of our knowledge has not been performed for existing generalizations of the Boltzmann equation to time-dependent settings [51, 52]. We note that our approach requires no assumptions on the time-periodicity of the Hamiltonian or the adiabaticity of the drive.

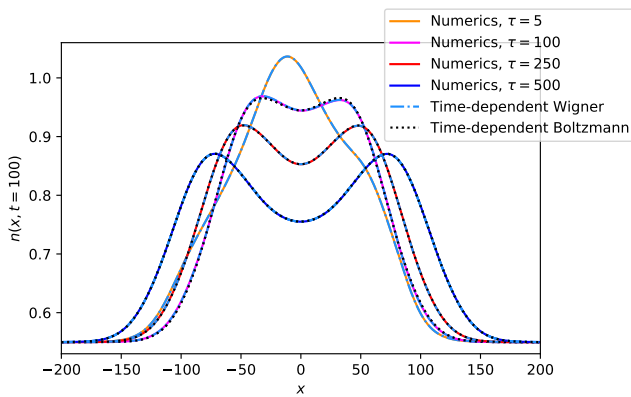


FIG. 3. Numerical time evolution of an initially localized charge density under the periodic time evolution in Eq. (68) after a time $t = 100$, for different driving periods $\tau = 5, 100, 250, 500$, compared to time-dependent Wigner function predictions (light blue dashed lines) and time-dependent Boltzmann predictions (black dotted lines), see text for further details. The time-dependent Boltzmann equation works well for timescales $\tau \gtrsim t$ but “freezes” for $\tau \lesssim t$, ceasing to provide an accurate description of the dynamics (the Boltzmann predictions for $\tau = 100$ and $\tau = 5$ are indistinguishable by eye). In contrast, the time-dependent Wigner function yields extremely accurate results over two orders of magnitude of driving periods.

A. Pumping local equilibrium states

The naïve generalization of the Boltzmann equation (49) to the time-dependent case reads

$$\partial_t \rho_n + \mathbf{v}_n(\mathbf{k}, t) \cdot \partial_{\mathbf{x}} \rho_n = 0, \quad (64)$$

where the group velocities for each band $\mathbf{v}_n(\mathbf{k}, t) := \partial_{\mathbf{k}} E_n(\mathbf{k}, t)$ now depend on time, initial data for local equilibrium states is again specified by Eq. (52) and predictions for the dynamics of the local charge density $n(\mathbf{x}, t)$ are again obtained from Eq. (53). Analogous equations with \mathbf{v}_n replaced by a time-dependent quasiparticle velocity have been found to perform well for time-dependent and instantaneously quantum integrable Hamiltonians in one spatial dimension [57].

We can justify this prescription microscopically and in local equilibrium by repeating the arguments of Section III B. We find that starting from a local equilibrium state at time t , Eq. (35) implies that the diagonal components of the band Wigner function $\tilde{w}(\mathbf{x}, \mathbf{k}, t) = U^\dagger(\mathbf{k}, t) w(\mathbf{x}, \mathbf{k}, t) U(\mathbf{k}, t)$ evolve instantaneously according to the time-dependent Boltzmann equation

$$\partial_t \tilde{w}_{nn}(\mathbf{x}, \mathbf{k}, t) + \mathbf{v}_n(\mathbf{k}, t) \cdot \partial_{\mathbf{x}} \tilde{w}_{nn}(\mathbf{x}, \mathbf{k}, t) = 0. \quad (65)$$

As in the time-independent case, the naïve Boltzmann prediction Eq. (64) is recovered once we make the identification $\tilde{w}_{nn}(\mathbf{x}, \mathbf{k}, t) \leftrightarrow \rho_n(\mathbf{x}, \mathbf{k}, t)$.

By the method of characteristics [58], Eq. (64) has an exact solution using coordinates $\mathbf{x}_n(\mathbf{k}, t)$ that solve the

initial value problem

$$\partial_t \mathbf{x}_n(\mathbf{k}, t) = \mathbf{v}_n(\mathbf{k}, t), \quad \mathbf{x}_n(\mathbf{k}, 0) = 0, \quad (66)$$

in terms of which the solution to the initial value problem for Eq. (64) reads

$$\rho_n(\mathbf{x}, \mathbf{k}, t) = \rho_n(\mathbf{x} - \mathbf{x}_n(\mathbf{k}, t), \mathbf{k}, 0). \quad (67)$$

In order to test this prediction numerically, we simulate the well-studied periodically-driven Rice-Mele Hamiltonian

$$\begin{aligned} \hat{H}_0(t) = \sum_{j=-L/2}^{L/2-1} & (J(t) \hat{c}_{j,A}^\dagger \hat{c}_{j,B} + \hat{c}_{j,A}^\dagger \hat{c}_{j+1,B} + \text{h.c.}) \\ & + \Delta(t) (\hat{c}_{j,A}^\dagger \hat{c}_{j,A} - \hat{c}_{j,B}^\dagger \hat{c}_{j,B}), \end{aligned} \quad (68)$$

where $J(t) = m + \cos(2\pi t/\tau)$ and $\Delta(t) = \sin(2\pi t/\tau)$, and the parameters m and τ will be varied. The Bloch Hamiltonian is given by

$$h(k, t) = \begin{pmatrix} \Delta(t) & J(t) + e^{ik} \\ J(t) + e^{-ik} & -\Delta(t) \end{pmatrix} \quad (69)$$

and the instantaneous band structure is $E_{\pm}(k, t) = \pm \sqrt{\Delta(t)^2 + J(t)^2 + 2J(t) \cos k} + 1$. For parameter values $0 < m < 2$, this Hamiltonian has unit winding number in the $J - \Delta$ plane about the gap-closing point $\Delta = J - 1 = 0$, implying Thouless pumping of one topologically quantized unit of charge per cycle in the adiabatic limit $\tau \rightarrow \infty$ at half filling and zero temperature [34]. In practice, $\beta, \tau < \infty$ and perfect topological quantization is lost [59].

As in the previous section, the Heisenberg-picture charge density operator $\hat{n}_j = \hat{c}_{j,A}^\dagger \hat{c}_{j,A} + \hat{c}_{j,B}^\dagger \hat{c}_{j,B}$ satisfies the microscopic continuity equation in Eq. (60) for all times, where now the current density operator $\hat{j}_j = i(\hat{c}_{j-1,A}^\dagger \hat{c}_{j,B} - \hat{c}_{j,B}^\dagger \hat{c}_{j-1,A})$. Thus the total charge current $\hat{J}(t) = \sum_{j=-L/2}^{L/2-1} \hat{j}_j$ recovers Eq. (8) in the thermodynamic limit as $L \rightarrow \infty$.

Before addressing in detail the question of whether orbital Wigner functions can capture inherently topological effects such as Thouless pumping, we first investigate how far Eq. (64) captures the nonequilibrium dynamics of charge under time evolution by the Hamiltonian in Eq. (68) away from half filling and at nonzero temperature. Initial conditions for the numerical simulations have the same form as in Sec. III B for the initial Hamiltonian $\hat{H}_0(0)$, with $L = 400$ sites, constant initial temperature $\beta = 1$ and inhomogeneous initial chemical potential as given in Eq. (61) with length scale $l = 40$, and bulk and central chemical potentials set to $\mu_0 = -2$ and $\mu_1 = 2$ respectively. We fix the simulation time to be $t = 100$ and vary the period of oscillation of the Hamiltonian over two orders of magnitude, from $\tau = 5$ to $\tau = 500$. In order to obtain these predictions, we (i) use a converged discretization of the time-evolution operator in the basis of single-particle Bloch states to obtain microscopic free-fermion predictions, (ii) integrate

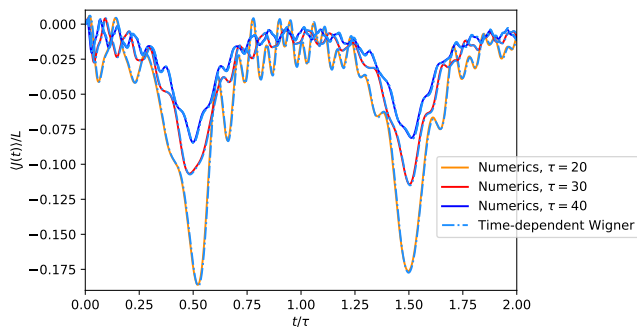


FIG. 4. Numerical time evolution of the current density under translation invariant Thouless pumping at inverse temperature $\beta = 100$. We simulate various time periods $\tau = 20, 30, 40$ and depict numerically obtained free-fermion predictions for the expected value of the current density operator $\langle \hat{j}_{j=0}(t) \rangle = \langle \hat{J}(t) \rangle / L$ at a given site (solid lines) against Wigner function predictions from Eq. (35) over two time periods (blue dashed lines). By translation invariance, these two quantities should be exactly equal in the thermodynamic limit, which is consistent with the results shown.

the characteristic equations (66) numerically to solve the time-dependent Boltzmann equation, and (iii) continue to solve the transport equation (35) using the staggered leapfrog method [53], now including time dependence of the Bloch Hamiltonian at each time step. Note that these methods are all applicable to arbitrary time dependence beyond periodic driving.

We find excellent agreement with the time-dependent Boltzmann equation in Eq. (64) in the regime $\tau \gtrsim t$ but marked discrepancies in the regime $\tau \ll t$, see Fig. 3. In particular, the time-dependent Boltzmann description appears to “freeze” as τ is decreased below the longest simulation time and yields an increasingly poor description of the dynamics as $\tau \rightarrow 0$. However, the time-dependent Wigner function dynamics in Eq. (35) continues to perform remarkably well even for short oscillation periods, with negligible ($< 0.1\%$) error in the predicted charge density for all drive periods simulated.

B. Thouless pumping

We now consider the periodically driven Rice-Mele model given in Eq. (68) at half filling $\mu = 0$, while varying the inverse temperature β and the driving period τ . The canonical theoretical setting [34] for Thouless pumping is recovered in the adiabatic, zero temperature limit, $\tau, \beta \rightarrow \infty$. In practice, $\tau, \beta < \infty$ and there are two natural ways to probe charge pumping via variation of Hamiltonian parameters.

The first approach, which should be feasible in experiments capable of imaging correlation functions between neighbouring unit cells, is to consider translation-invariant initial states and study the dynamics of the total charge current $\langle \hat{J}(t) \rangle$ directly. This approach is best

sued for demonstrating theoretically that Eq. (35) can capture Thouless pumping exactly in the adiabatic limit, see Eq. (73) below.

An alternative approach mimics experimental tests of Thouless pumping in ultracold atoms [60] and consists of initializing a localized lump of charge, as in Eq. (61), before applying a slow variation of Hamiltonian parameters to induce pumping. We find that Eq. (35) accurately captures such charge dynamics over multiple pumping cycles.

It is worth noting that the time-dependent Boltzmann equation in Eq. (64) is completely inadequate for describing Thouless pumping, because it is invariant under spatial reflection and therefore predicts that for parity-even initial conditions, $\langle \hat{J}(t) \rangle = 0$ for all time. Put differently, the non-zero current generated dynamically by Thouless pumping is incompatible with the assumption of instantaneous local equilibrium in Eq. (55), which can never yield a current-carrying state.

1. Inducing a translation-invariant current

We first consider the translation-invariant setting, in which a slow variation of Hamiltonian parameters induces a homogeneous, non-zero current in the system. Because of translation invariance, neither higher-order spatial derivative corrections to Eq. (35), nor corrections to the initial local density approximation in Eq. (25) can arise, so that the transport formalism given by Eqs. (25) and (35) becomes exact in the thermodynamic limit.

Concretely, we let the initial density matrix $\hat{\rho} \propto e^{-\beta \hat{H}_0(0)}$ and fix τ . By translation invariance, the exact transport equation for the Wigner function takes the simple form

$$\partial_t w(k, t) = -i[h(k, t), w(k, t)] \quad (70)$$

where $w(x, k, t) = w(k, t)$ and the initial condition

$$w(k, 0) = \frac{1}{1 + e^{\beta h(k, 0)}}. \quad (71)$$

is also exact. Defining the single-particle propagator as the time-ordered exponential $U(k, t) = \mathcal{T} \exp\left(-i \int_0^t dt' h(k, t')\right)$, it follows that

$$w(k, t) = U(k, t) w(k, 0) U^\dagger(k, t). \quad (72)$$

We then expect by the identity in Eq. (16) that

$$\langle \hat{J}(t) \rangle / L \sim \int_{\text{BZ}} \frac{dk}{V_{\text{BZ}}} \sum_{\alpha, \beta=1}^M \partial_k h_{\alpha\beta}(k) w_{\beta\alpha}(k, t) \quad (73)$$

holds exactly in the thermodynamic limit. Thus, Eq. (35) should accurately capture Thouless pumping in finite, translation invariant systems for all temperatures β and driving periods τ , up to finite-size corrections. Although

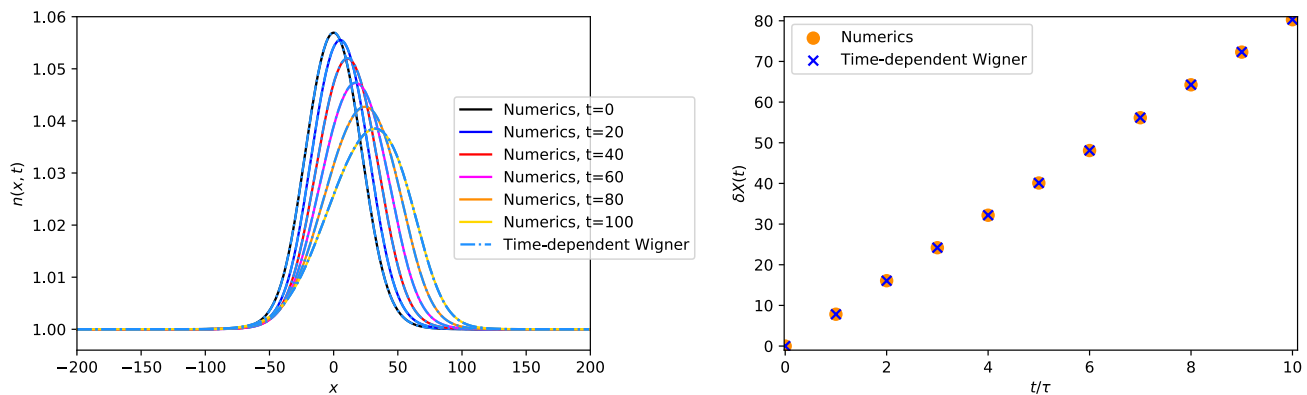


FIG. 5. **Left:** Numerical time evolution of an initially localized charge density under the periodic time evolution Eq. (68) for a time $t = 100$ and driving period $\tau = 10$ compared to time-dependent Wigner function predictions (light blue dashed lines). The bulk temperature $\beta = 10$ and the initial condition is as in Eq. (61) with bulk chemical potential $\mu_0 = 0$, central chemical potential $\mu_1 = 1$ and characteristic width $l = 80$. **Right:** The evolution of the first moment of charge density resulting from the dynamics on the left. The agreement between free-fermion numerics (orange dots) and Wigner function predictions (blue crosses) is excellent.

it is arguably redundant, we verify this numerically in Fig. 4 by comparing the expectation value of the microscopic current density operator at a single site $\langle \hat{j}_{j=0}(t) \rangle$ against numerical integration of Eq. (73), for $L = 400$ sites, inverse temperature $\beta = 100$ and various finite driving periods. Since the resulting dynamics is rather intricate, we restrict the simulation time to two driving periods for clarity and the agreement is excellent as expected.

2. Pumping an inhomogeneous charge density

We next consider pumping an initial, localized charge density in local equilibrium, which can be seen as a hydrodynamic version of the initial conditions realized experimentally in Ref. [60]. We set the bulk temperature $\beta = 10$ to be relatively low and consider an inhomogeneous chemical potential as in Eq. (61) with length scale $l = 80$. We set the bulk chemical potential to half filling, $\mu_0 = 0$ and the central chemical potential to $\mu_1 = 1$. We let the driving period $\tau = 10$ and simulate times up to $t = 100$, i.e. ten driving periods. This should be far from adiabaticity and thus provide an especially stringent test of Eq. (35). To highlight the physics of charge pumping, we further compute the evolution of the first moment of the charge density

$$\delta X(t) = \sum_{x=-L/2}^{L/2-1} x [n(x,t) - n(x,0)] \quad (74)$$

as a function of time, which grows linearly at a rate set by the initial conditions. Once again the agreement between theory and numerics is excellent, see Fig. 5.

C. Charge transport from instantaneously flat bands

As a final example, we consider the propagation of charge in stroboscopically driven SSH chains. This example is particularly striking because the group velocity of each quasiparticle vanishes instantaneously, but charge nevertheless spreads ballistically. Specifically, we consider evolution under the time-periodic Hamiltonian

$$\hat{H}_0(t) = \begin{cases} \hat{H}_{\text{trivial}}, & n\tau \leq t < (n + \frac{1}{2})\tau, \\ \hat{H}_{\text{topological}}, & (n + \frac{1}{2})\tau \leq t < (n + 1)\tau, \end{cases} \quad (75)$$

for $n = 0, 1, 2, \dots$, where

$$\begin{aligned} \hat{H}_{\text{trivial}} &= \sum_{j=-L/2}^{L/2-1} \hat{c}_{j,B}^\dagger \hat{c}_{j,A} + \text{h.c.}, \\ \hat{H}_{\text{topological}} &= \sum_{j=-L/2}^{L/2-1} \hat{c}_{j+1,A}^\dagger \hat{c}_{j,B} + \text{h.c.}, \end{aligned} \quad (76)$$

and τ denotes the driving period. This model alternates stroboscopically between the two “trivial” and “topological” dimerized limits of the usual SSH model [61]. (We note that various versions of this driven system have arisen before in the context of time-crystal physics [62–65], though the latter is unrelated to our focus here.) According to the semiclassical theory of transport, both the Hamiltonians \hat{H}_{trivial} and $\hat{H}_{\text{topological}}$ are insulating, with flat-band spectra $E_1(k) = -E_2(k) = 1$ for all k and thus vanishing group velocities in each band.

Thus the time-dependent Boltzmann equation (64), which assumes instantaneous local equilibrium, would predict no dynamics at all. However, a local equilibrium state with respect to \hat{H}_{trivial} will be far from equilibrium

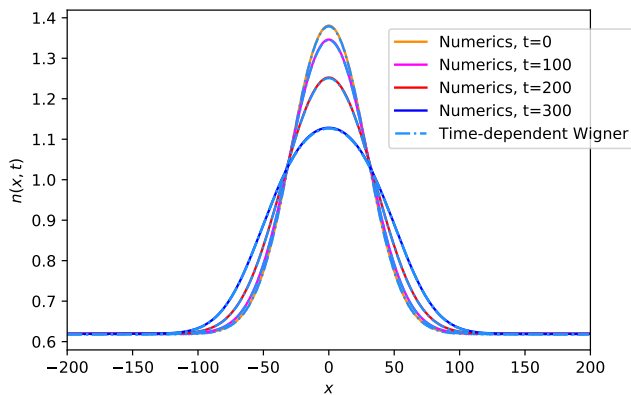


FIG. 6. Numerical time evolution of the charge density for the periodically driven SSH model Eq. (75) with driving period $\tau = 5$, whose bands are always instantaneously flat. The drive nevertheless enables ballistic charge spreading that is accurately captured by the Wigner function prediction Eq. (35). The initial condition is as in Eq. (61) with $\beta = 1$, $\mu_0 = -1$, $\mu_1 = 1$ and $l = 40$ and agreement persists over sixty driving periods.

with respect to $\hat{H}_{\text{topological}}$ and the resulting quench-like dynamics turns out to be sufficient to yield ballistic spreading of charge. (This possibility could also have been deduced from the presence of band-curvature in the Floquet-Bloch spectrum for this model [65] in a Floquet-Boltzmann approach [51, 52].)

The resulting dynamics is straightforwardly captured by Eq. (35) with the stroboscopic Bloch Hamiltonian

$$h(k, t) = \begin{cases} h_{\text{trivial}}(k), & n\tau \leq t < (n + \frac{1}{2})\tau, \\ h_{\text{topological}}(k), & (n + \frac{1}{2})\tau \leq t < (n + 1)\tau, \end{cases} \quad (77)$$

where

$$h_{\text{trivial}}(k) = \begin{pmatrix} 0 & 1 \\ 1 & 0 \end{pmatrix}, \quad h_{\text{topological}}(k) = \begin{pmatrix} 0 & e^{-ik} \\ e^{ik} & 0 \end{pmatrix}. \quad (78)$$

To test the orbital Wigner function predictions numerically, we prepare charge-spot initial conditions (61) with $\mu_0 = -1$, $\mu_1 = 1$, bulk inverse temperature $\beta = 1$ and length scale $l = 40$ for the Hamiltonian \hat{H}_{trivial} on $L = 400$ sites, before subjecting this to periodic driving as in Eq. (75) with driving period $\tau = 5$. See Fig. 6 for a comparison between free-fermion numerics and the numerical solution to Eq. (35). We note that the discontinuous dynamics in Eq. (75) makes convergence of both the free-fermion numerics and Wigner function dynamics particularly challenging in this case, but once it is achieved the agreement is once again excellent.

V. DISCUSSION

We have presented an analytically transparent and numerically tractable theory of coherent electron transport in stationary and driven multiband (and more generally multiorbital) crystals. Our proposed formalism accurately captures far-from-equilibrium charge and current densities arising from non-uniform and quantum coherent initial conditions. We illustrated this point by simulating multiple distinct experimentally accessible Hamiltonians and various kinds of dynamics beyond standard semiclassical transport theory. While this work focuses primarily on electric charge and current density, our approach allows for straightforward generalizations to spin, thermal, and thermoelectric transport, through evaluating the corresponding charge and current operators from the orbital Wigner function.

Although we have chosen to highlight the rich physics that can arise in multiband systems even in the absence of interactions and disorder, any practically useful transport theory must be able to model the dissipative hydrodynamic behavior that arises in realistic physical systems. On this front, recent work on one-dimensional systems has shown that the venerable quantum Boltzmann equation can yield remarkably quantitatively accurate results even in strong-coupling, long-time regimes [66–68], beyond the weak-coupling, short-time regime in which quantum kinetic theory might rigorously be expected to hold [69, 70]. This raises the tantalizing possibility of a transport theory of interacting multiband systems with a comparable degree of quantitative accuracy to the results presented here. We note that the collision terms appearing in the resulting equations would naturally be matrix-valued [70], and to that extent differ from standard formulations of the quantum Boltzmann equation with possibly non-trivial implications for hydrodynamics and transport. We leave a deeper investigation of this fascinating question for future work.

A proper treatment of interactions will be necessary to obtain meaningful predictions for both linear and nonlinear conductivities and optical response from orbital Wigner functions. In this setting, it would be interesting to understand how far systematic derivations of the collision integral, along the lines sketched above, can capture non-trivial corrections to semiclassical transport theory. For example, the inclusion of a real-space shift during scattering events [71, 72] was found to be necessary to yield a collision integral consistent with quantum kinetic theory at nonlinear order in the applied electric field [73, 74]. Similarly, off-diagonal contributions to the position operator [43–45] are commonly neglected in tight-binding descriptions of condensed-matter systems but can nevertheless play an important role in nonlinear optical response. Such corrections could in principle be captured in our approach by a suitable modification of the two-body operators corresponding to the center of charge and the electrostatic potential energy.

Thus orbital Wigner functions could provide a new,

microscopic route towards deriving nonlinear response functions in settings where quantum coherence is important. Indeed, the fact that orbital Wigner functions correctly account for the plethora of quantum coherent effects studied in this paper strongly suggests that they can accurately capture other known topological and geometrical transport phenomena that arise in multiband systems, such as the Berry phase and the anomalous velocity [75]. As an illustrative example, our approach effortlessly handles band crossings and near-degenerate bands, which can be challenging to treat using standard Boltzmann-type techniques.

While we expect that our formalism encompasses these well-known physical phenomena, we emphasize that it also has the capacity to predict new ones. Recent results on Floquet theory [76], non-linear optical responses [74, 77–79], and light-matter coupling [80, 81] raise the possibility that new and possibly unforeseen geometric invariants could play an essential role in non-equilibrium transport in both Hamiltonian and driven systems. The systematic approach pursued in these works and in the current paper suggest one potential strategy for identifying the most promising lattice systems and initial conditions for unconventional quantum-coherent transport to arise, for example, in flat-band systems [82–85]. Looking beyond solid-state platforms, the numerical accuracy promised by our approach makes it ideally suited for a direct quantitative comparison with analogue quantum simulators [35, 59, 86, 87], with the potential to both reveal shortcomings in their theoretical description and also point to new physics.

More generally, Wigner-function-based approaches

have recently been applied successfully in contexts ranging from thermal transport [88, 89] to bosonic systems [90] and the bosonization of Fermi surfaces [91, 92], and it might be fruitful to connect these proposals to the approach taken here. While we do not expect the full gamut of possibilities for electron transport in crystals to succumb to the formalism outlined in this paper, a broader lesson from our work is that most conventional theories of transport are inadequate for confronting the sheer variety of large-scale dynamics that can arise even in minimal tight-binding models. Attaining quantitative accuracy in this simplest of settings, as we have sought to do here, strikes us as a prerequisite for developing a theory of transport in solids that is equipped to address the many long-standing challenges in this field.

ACKNOWLEDGMENTS

We thank Alexander Avdoshkin, Pieter W. Claeys, Frank Schindler, Thaís V. Trevisan, and Christopher W. Wächtler for stimulating discussions, and Nick G. Jones and Ruben Verresen for collaboration on related work. J. M. was supported by the German National Academy of Sciences Leopoldina through Grant No. LPDS 2022-06 and, in part, by the Deutsche Forschungsgemeinschaft under Grant cluster of excellence ct.qmat (EXC 2147, Project No. 390858490). Work by D.S.B. and J.E.M. was supported by the MURI project TOPFORCE of the Air Force Office of Scientific Research (AFSOR) under grant number FA9550-22-1-027.

-
- [1] M.-C. Chang and Q. Niu, Berry phase, hyperorbits, and the hofstadter spectrum, *Physical Review Letters* **75**, 1348–1351 (1995).
 - [2] M.-C. Chang and Q. Niu, Berry phase, hyperorbits, and the hofstadter spectrum: Semiclassical dynamics in magnetic bloch bands, *Physical Review B* **53**, 7010–7023 (1996).
 - [3] G. Sundaram and Q. Niu, Wave-packet dynamics in slowly perturbed crystals: Gradient corrections and berry-phase effects, *Physical Review B* **59**, 14915 (1999).
 - [4] R. Karplus and J. Luttinger, Hall effect in ferromagnetics, *Physical Review* **95**, 1154 (1954).
 - [5] T. Jungwirth, Q. Niu, and A. MacDonald, Anomalous hall effect in ferromagnetic semiconductors, *Physical review letters* **88**, 207208 (2002).
 - [6] N. A. Sinitsyn, Semiclassical theories of the anomalous hall effect, *Journal of Physics: Condensed Matter* **20**, 023201 (2007).
 - [7] N. Nagaosa, J. Sinova, S. Onoda, A. H. MacDonald, and N. P. Ong, Anomalous hall effect, *Reviews of modern physics* **82**, 1539 (2010).
 - [8] N. Ashcroft and N. Mermin, *Solid State Physics*, HRW international editions (Holt, Rinehart and Winston, 1976).
 - [9] D. Culcer, Y. Yao, and Q. Niu, Coherent wave-packet evolution in coupled bands, *Physical Review B—Condensed Matter and Materials Physics* **72**, 085110 (2005).
 - [10] R. Shindou and K.-I. Imura, Noncommutative geometry and non-abelian berry phase in the wave-packet dynamics of bloch electrons, *Nuclear Physics B* **720**, 399 (2005).
 - [11] T. Stedman and L. M. Woods, Transport theory within a generalized Boltzmann equation for multiband wave packets, *Phys. Rev. Res.* **2**, 033086 (2020).
 - [12] L. Demeio, L. Barletti, A. Bertoni, P. Bordone, and C. Jacoboni, Wigner-function approach to multiband transport in semiconductors, *Physica B: Condensed Matter* **314**, 104 (2002).
 - [13] M. B. Unlu, B. Rosen, H.-L. Cui, and P. Zhao, Multiband wigner function formulation of quantum transport, *Physics Letters A* **327**, 230 (2004).
 - [14] D. Culcer and Q. Niu, Geometrical phase effects on the Wigner distribution of Bloch electrons, *Phys. Rev. B* **74**, 035209 (2006).
 - [15] D. Culcer, M. E. Lucassen, R. A. Duine, and R. Winkler, Current-induced spin torques in III-V ferromagnetic semiconductors, *Phys. Rev. B* **79**, 155208 (2009).
 - [16] O. Morandi, Multiband Wigner-function formalism ap-

- plied to the Zener band transition in a semiconductor, *Phys. Rev. B* **80**, 024301 (2009).
- [17] C. H. Wong and Y. Tserkovnyak, Quantum kinetic equation in phase-space textured multiband systems, *Phys. Rev. B* **84**, 115209 (2011).
- [18] C. Wickles and W. Belzig, Effective quantum theories for Bloch dynamics in inhomogeneous systems with nontrivial band structure, *Phys. Rev. B* **88**, 045308 (2013).
- [19] K. Morawetz, Kinetic theory of spin-polarized systems in electric and magnetic fields with spin-orbit coupling. I. Kinetic equation and anomalous Hall and spin-Hall effects, *Phys. Rev. B* **92**, 245425 (2015).
- [20] G. J. Iafrate, V. N. Sokolov, and J. B. Krieger, Quantum transport and the Wigner distribution function for Bloch electrons in spatially homogeneous electric and magnetic fields, *Phys. Rev. B* **96**, 144303 (2017).
- [21] A. Sekine, D. Culcer, and A. H. MacDonald, Quantum kinetic theory of the chiral anomaly, *Phys. Rev. B* **96**, 235134 (2017).
- [22] A. Cepellotti and B. Kozinsky, Interband tunneling effects on materials transport properties using the first principles wigner distribution, *Materials Today Physics* **19**, 100412 (2021).
- [23] P. Bhalla, M.-X. Deng, R.-Q. Wang, L. Wang, and D. Culcer, Nonlinear ballistic response of quantum spin Hall edge states, *Phys. Rev. Lett.* **127**, 206801 (2021).
- [24] E. J. König and A. Levchenko, Quantum kinetics of anomalous and nonlinear hall effects in topological semimetals, *Annals of Physics* **435**, 168492 (2021), special issue on Philip W. Anderson.
- [25] T. Valet and R. Raimondi, Semiclassical kinetic theory for systems with non-trivial quantum geometry and the expectation value of physical quantities, *Europhysics Letters* **143**, 26004 (2023).
- [26] J. Irving and R. W. Zwanzig, The statistical mechanical theory of transport processes. V. Quantum hydrodynamics, *The Journal of Chemical Physics* **19**, 1173 (1951).
- [27] M. Hinarejos, A. Pérez, and M.-C. Bañuls, Wigner function for a particle in an infinite lattice, *New Journal of Physics* **14**, 103009 (2012).
- [28] M. Fagotti, Higher-order generalized hydrodynamics in one dimension: The noninteracting test, *Physical Review B* **96**, 220302 (2017).
- [29] A. Bastianello and A. De Luca, Nonequilibrium steady state generated by a moving defect: The supersonic threshold, *Physical Review Letters* **120**, 10.1103/physrevlett.120.060602 (2018).
- [30] M. Fagotti, Locally quasi-stationary states in noninteracting spin chains, *SciPost Physics* **8**, 10.21468/scipostphys.8.3.048 (2020).
- [31] M. Coppola, G. T. Landi, and D. Karevski, Wigner dynamics for quantum gases under inhomogeneous gain and loss processes with dephasing, *Physical Review A* **107**, 10.1103/physreva.107.052213 (2023).
- [32] F. H. Essler, A short introduction to generalized hydrodynamics, *Physica A: Statistical Mechanics and its Applications* **631**, 127572 (2023).
- [33] M. Hinarejos, M. C. Bañuls, and A. Pérez, Wigner formalism for a particle on an infinite lattice: dynamics and spin, *New Journal of Physics* **17**, 013037 (2015).
- [34] D. Thouless, Quantization of particle transport, *Physical Review B* **27**, 6083 (1983).
- [35] P. T. Brown, D. Mitra, E. Guardado-Sanchez, R. Nourafkan, A. Reymbaut, C.-D. Hébert, S. Bergeron, A.-M. S. Tremblay, J. Kokalj, D. A. Huse, P. Schauf, and W. S. Bakr, Bad metallic transport in a cold atom Fermi-Hubbard system, *Science* **363**, 379–382 (2019).
- [36] M. Schemmer, I. Bouchoule, B. Doyon, and J. Dubail, Generalized hydrodynamics on an atom chip, *Phys. Rev. Lett.* **122**, 090601 (2019).
- [37] E. Guardado-Sanchez, A. Morningstar, B. M. Spar, P. T. Brown, D. A. Huse, and W. S. Bakr, Subdiffusion and Heat Transport in a Tilted Two-Dimensional Fermi-Hubbard System, *Phys. Rev. X* **10**, 011042 (2020).
- [38] C. Gross and W. S. Bakr, Quantum gas microscopy for single atom and spin detection, *Nature Physics* **17**, 1316–1323 (2021).
- [39] N. Malvania, Y. Zhang, Y. Le, J. Dubail, M. Rigol, and D. S. Weiss, Generalized hydrodynamics in strongly interacting 1D Bose gases, *Science* **373**, 1129–1133 (2021).
- [40] D. Wei, A. Rubio-Abadal, B. Ye, F. Machado, J. Kemp, K. Srakaew, S. Hollerith, J. Rui, S. Gopalakrishnan, N. Y. Yao, I. Bloch, and J. Zeiher, Quantum gas microscopy of Kardar-Parisi-Zhang superdiffusion, *Science* **376**, 716–720 (2022).
- [41] S. Brandstetter, P. Lunt, C. Heintze, G. Giacalone, L. H. Heyen, M. Gałka, K. Subramanian, M. Holtén, P. M. Preiss, S. Floerchinger, and S. Jochim, Emergent interaction-driven elliptic flow of few fermionic atoms, *Nature Physics* **10.1038/s41567-024-02705-8** (2025).
- [42] H. Spohn, *Large scale dynamics of interacting particles* (Springer Science & Business Media, 2012).
- [43] T. G. Pedersen, K. Pedersen, and T. Brun Kristensen, Optical matrix elements in tight-binding calculations, *Phys. Rev. B* **63**, 201101 (2001).
- [44] T. Sandu, Optical matrix elements in tight-binding models with overlap, *Phys. Rev. B* **72**, 125105 (2005).
- [45] J. Ibañez-Azpiroz, F. de Juan, and I. Souza, Assessing the role of interatomic position matrix elements in tight-binding calculations of optical properties, *SciPost Physics* **12**, 10.21468/scipostphys.12.2.070 (2022).
- [46] M. Fagotti and V. Marić, Asymptotic behaviour of determinants through the expansion of theoyal star product (2024), [arXiv:2406.12781 \[math-ph\]](https://arxiv.org/abs/2406.12781).
- [47] B. Santra, C. Baals, R. Labouvie, A. B. Bhattacharjee, A. Pelster, and H. Ott, Measuring finite-range phase coherence in an optical lattice using talbot interferometry, *Nature Communications* **8**, 10.1038/ncomms15601 (2017).
- [48] P. A. Murthy and S. Jochim, Direct imaging of the order parameter of an atomic superfluid using matterwave optics (2019), [arXiv:1911.10824 \[cond-mat.quant-gas\]](https://arxiv.org/abs/1911.10824).
- [49] J. C. Brüggengjürgen, M. S. Fischer, and C. Weitenberg, A phase microscope for quantum gases, *arXiv preprint arXiv:2410.10611* (2024).
- [50] K. Yang, W. Paul, S.-H. Phark, P. Willke, Y. Bae, T. Choi, T. Esat, A. Ardavan, A. J. Heinrich, and C. P. Lutz, Coherent spin manipulation of individual atoms on a surface, *Science* **366**, 509 (2019).
- [51] M. Genske and A. Rosch, Floquet-boltzmann equation for periodically driven fermi systems, *Physical Review A* **92**, 10.1103/physreva.92.062108 (2015).
- [52] I. Esin, M. S. Rudner, G. Refael, and N. H. Lindner, Quantized transport and steady states of floquet topological insulators, *Phys. Rev. B* **97**, 245401 (2018).
- [53] W. H. Press, *Numerical recipes 3rd edition: The art of scientific computing* (Cambridge university press, 2007).
- [54] S.-A. Cheong and C. L. Henley, Many-body density ma-

- trices for free fermions, *Physical Review B* **69**, 075111 (2004).
- [55] I. Peschel, Calculation of reduced density matrices from correlation functions, *Journal of Physics A: Mathematical and General* **36**, L205 (2003).
- [56] A. Mitra, Quantum quench dynamics, *Annual Review of Condensed Matter Physics* **9**, 245 (2018).
- [57] A. Bastianello, V. Alba, and J.-S. Caux, Generalized hydrodynamics with space-time inhomogeneous interactions, *Physical Review Letters* **123**, 10.1103/physrevlett.123.130602 (2019).
- [58] R. Courant and D. Hilbert, *Methods of Mathematical Physics, Volume 2* (John Wiley & Sons, 2024).
- [59] R. Citro and M. Aidelsburger, Thouless pumping and topology, *Nature Reviews Physics* **5**, 87–101 (2023).
- [60] S. Nakajima, T. Tomita, S. Taie, T. Ichinose, H. Ozawa, L. Wang, M. Troyer, and Y. Takahashi, Topological thouless pumping of ultracold fermions, *Nature Physics* **12**, 296 (2016).
- [61] W.-P. Su, J. Schrieffer, and A. Heeger, Soliton excitations in polyacetylene, *Physical Review B* **22**, 2099 (1980).
- [62] V. Khemani, A. Lazarides, R. Moessner, and S. L. Sondhi, Phase structure of driven quantum systems, *Phys. Rev. Lett.* **116**, 250401 (2016).
- [63] C. W. von Keyserlingk and S. L. Sondhi, Phase structure of one-dimensional interacting floquet systems. i. abelian symmetry-protected topological phases, *Phys. Rev. B* **93**, 245145 (2016).
- [64] A. C. Potter, T. Morimoto, and A. Vishwanath, Classification of interacting topological floquet phases in one dimension, *Phys. Rev. X* **6**, 041001 (2016).
- [65] T. Iadecola, S. Sen, and L. Sivertsen, Floquet insulators and lattice fermions, *Phys. Rev. Lett.* **132**, 136601 (2024).
- [66] B. Bertini, F. H. L. Essler, S. Groha, and N. J. Robinson, Prethermalization and Thermalization in Models with Weak Integrability Breaking, *Phys. Rev. Lett.* **115**, 180601 (2015).
- [67] B. Bertini, F. H. Essler, S. Groha, and N. J. Robinson, Thermalization and light cones in a model with weak integrability breaking, *Physical Review B* **94**, 245117 (2016).
- [68] P. Zechmann, A. Bastianello, and M. Knap, Tunable transport in the mass-imbalanced fermi-hubbard model, *Physical Review B* **106**, 075115 (2022).
- [69] L. Erdős, M. Salmhofer, and H.-T. Yau, On the quantum boltzmann equation, *Journal of statistical physics* **116**, 367 (2004).
- [70] M. L. R. Fürst, C. B. Mendl, and H. Spohn, Matrix-valued boltzmann equation for the hubbard chain, *Phys. Rev. E* **86**, 031122 (2012).
- [71] M.-C. Chang and Q. Niu, Berry phase, hyperorbits, and the hofstadter spectrum: Semiclassical dynamics in magnetic bloch bands, *Phys. Rev. B* **53**, 7010 (1996).
- [72] C. Xiao, Z. Z. Du, and Q. Niu, Theory of nonlinear Hall effects: Modified semiclassics from quantum kinetics, *Phys. Rev. B* **100**, 165422 (2019).
- [73] Y. Gao, Semiclassical dynamics and nonlinear charge current, *Front. Phys.* **14**, 33404 (2019).
- [74] D. Kaplan, T. Holder, and B. Yan, Unifying semiclassics and quantum perturbation theory at nonlinear order, *SciPost Phys.* **14**, 082 (2023).
- [75] D. Xiao, M.-C. Chang, and Q. Niu, Berry phase effects on electronic properties, *Rev. Mod. Phys.* **82**, 1959 (2010).
- [76] P. M. Schindler and M. Bukov, *Geometric Floquet theory* (2025), [arXiv:2410.07029](https://arxiv.org/abs/2410.07029) [quant-ph].
- [77] J. Ahn, G.-Y. Guo, N. Nagaosa, and A. Vishwanath, Riemannian geometry of resonant optical responses, *Nature Physics* **18**, 290 (2022).
- [78] A. Avdoshkin, J. Mitscherling, and J. E. Moore, *The multi-state geometry of shift current and polarization* (2024), [arXiv:2409.16358](https://arxiv.org/abs/2409.16358) [cond-mat.str-el].
- [79] J. Mitscherling, A. Avdoshkin, and J. E. Moore, *Gauge-invariant projector calculus for quantum state geometry and applications to observables in crystals* (2024), [arXiv:2412.03637](https://arxiv.org/abs/2412.03637) [cond-mat.str-el].
- [80] T. Holder, D. Kaplan, and B. Yan, Consequences of time-reversal-symmetry breaking in the light-matter interaction: Berry curvature, quantum metric, and diabatic motion, *Phys. Rev. Res.* **2**, 033100 (2020).
- [81] G. E. Topp, C. J. Eckhardt, D. M. Kennes, M. A. Sentef, and P. Törmä, Light-matter coupling and quantum geometry in moiré materials, *Phys. Rev. B* **104**, 064306 (2021).
- [82] D. Leykam and S. Flach, Perspective: Photonic flatbands, *APL Photonics* **3**, 070901 (2018).
- [83] R. A. V. Poblete, Photonic flat band dynamics, *Advances in Physics: X* **6**, 1878057 (2021), <https://doi.org/10.1080/23746149.2021.1878057>.
- [84] J. Mitscherling and T. Holder, Bound on resistivity in flat-band materials due to the quantum metric, *Phys. Rev. B* **105**, 085154 (2022).
- [85] C. Danieli, A. Andreanov, D. Leykam, and S. Flach, *Flat band fine-tuning and its photonic applications* (2024), [arXiv:2403.17578](https://arxiv.org/abs/2403.17578) [physics.optics].
- [86] T. Ozawa, H. M. Price, A. Amo, N. Goldman, M. Hafezi, L. Lu, M. C. Rechtsman, D. Schuster, J. Simon, O. Zilberberg, and I. Carusotto, Topological photonics, *Rev. Mod. Phys.* **91**, 015006 (2019).
- [87] J. C. Halimeh, M. Aidelsburger, F. Grusdt, P. Hauke, and B. Yang, Cold-atom quantum simulators of gauge theories, *Nature Physics* **21**, 25 (2025).
- [88] M. Simoncelli, N. Marzari, and F. Mauri, Unified theory of thermal transport in crystals and glasses, *Nature Physics* **15**, 809 (2019).
- [89] M. Simoncelli, N. Marzari, and F. Mauri, Wigner formulation of thermal transport in solids, *Phys. Rev. X* **12**, 041011 (2022).
- [90] L. Mangeolle, L. Savary, and L. Balents, *Quantum kinetic equation and thermal conductivity tensor for bosons* (2024), [arXiv:2402.17329](https://arxiv.org/abs/2402.17329) [cond-mat.str-el].
- [91] L. V. Delacrétaz, Y.-H. Du, U. Mehta, and D. T. Son, Nonlinear bosonization of Fermi surfaces: The method of coadjoint orbits, *Phys. Rev. Res.* **4**, 033131 (2022).
- [92] T. Park and L. Balents, An exact method for bosonizing the Fermi surface in arbitrary dimensions, *SciPost Phys.* **16**, 069 (2024).
- [93] A. Paszke, S. Gross, S. Chintala, G. Chanan, E. Yang, Z. DeVito, Z. Lin, A. Desmaison, L. Antiga, and A. Lerer, Automatic differentiation in pytorch (2017).
- [94] J. P. Boyd, *Chebyshev and Fourier spectral methods* (Courier Corporation, 2001).

Appendix A: Fourier transform conventions

We define the Fourier transform of a function $f : \Lambda \rightarrow \mathbb{C}$ by

$$f(\mathbf{k}) = \sum_{j \in \Lambda} f(\mathbf{R}_j) e^{-i\mathbf{k} \cdot \mathbf{R}_j} \quad (\text{A1})$$

with inverse

$$f(\mathbf{R}_j) = \int_{\text{BZ}} \frac{d\mathbf{k}}{V_{\text{BZ}}} e^{i\mathbf{k} \cdot \mathbf{R}_j} f(\mathbf{k}), \quad (\text{A2})$$

where BZ denotes the first Brillouin zone and V_{BZ} its volume. Thus the (dual-lattice-periodic extension of the) Dirac delta function reads

$$\delta(\mathbf{k}) = \frac{1}{V_{\text{BZ}}} \sum_{j \in \Lambda} e^{-i\mathbf{k} \cdot \mathbf{R}_j} \quad (\text{A3})$$

while the real-space Kronecker delta can be written as

$$\delta_{\mathbf{R}_j, 0} = \int_{\text{BZ}} \frac{d\mathbf{k}}{V_{\text{BZ}}} e^{i\mathbf{k} \cdot \mathbf{R}_j}. \quad (\text{A4})$$

It will be useful to define the ‘‘Brillouin delta function’’

$$\delta_{\text{B}}(\mathbf{x}) = \int_{\text{BZ}} \frac{d\mathbf{k}}{V_{\text{BZ}}} e^{i\mathbf{k} \cdot \mathbf{x}} \quad (\text{A5})$$

for general incommensurate positions \mathbf{x} . Recall that this equals unity when $\mathbf{x} = \mathbf{0}$, vanishes for $\mathbf{x} \in \Lambda \setminus \mathbf{0}$, and resembles a product of sinc functions for general incommensurate \mathbf{x} .

We define momentum-space fermion operators by

$$\hat{c}_\alpha(\mathbf{k}) = \sum_{j \in \Lambda} e^{-i\mathbf{k} \cdot \mathbf{R}_{j\alpha}} \hat{c}_{j\alpha}, \quad (\text{A6})$$

which are easily verified to satisfy canonical anticommutation relations

$$\{\hat{c}_\alpha^\dagger(\mathbf{k}), \hat{c}_{\alpha'}(\mathbf{k}')\} = V_{\text{BZ}} \delta(\mathbf{k} - \mathbf{k}') \delta_{\alpha\alpha'} \quad (\text{A7})$$

and the inversion formula

$$\hat{c}_{j\alpha} = \int_{\text{BZ}} \frac{d\mathbf{k}}{V_{\text{BZ}}} e^{i\mathbf{k} \cdot \mathbf{R}_{j\alpha}} \hat{c}_\alpha(\mathbf{k}). \quad (\text{A8})$$

Appendix B: Higher-order derivative corrections

We now present the full set of derivative corrections to the transport equation Eq. (21) (i.e. due to evolution under \hat{H}_0 alone). Continuing the Taylor expansion of Eq. (20) to higher orders in $\partial_{\mathbf{x}}$ yields the expression

$$\partial_t \hat{W}_{\alpha\beta}(\mathbf{x}, \mathbf{k}, t) = \sum_{m=0}^{\infty} \frac{i^{m+1}}{m! 2^m} \sum_{\vec{i} \in \{1, 2, \dots, d\}^m} \sum_{\gamma=1}^M \partial_{k_{\vec{i}}}^{(m)} h_{\gamma\alpha}(\mathbf{k}) \partial_{x_{\vec{i}}}^{(m)} \hat{W}_{\gamma\beta}(\mathbf{x}, \mathbf{k}, t) - (-1)^m \partial_{k_{\vec{i}}}^{(m)} h_{\beta\gamma}(\mathbf{k}) \partial_{x_{\vec{i}}}^{(m)} \hat{W}_{\alpha\gamma}(\mathbf{x}, \mathbf{k}, t) \quad (\text{B1})$$

where in each term we use the notation $\partial_{k_{\vec{i}}}^{(m)} := \partial_{k_{i_1}} \partial_{k_{i_2}} \dots \partial_{k_{i_m}}$ and $\partial_{x_{\vec{i}}}^{(m)} := \partial_{x_{i_1}} \partial_{x_{i_2}} \dots \partial_{x_{i_m}}$ and $\vec{i} = (i_1, i_2, \dots, i_m)$ denotes the corresponding multi-index. It follows by linearity of this equation in \hat{W} that the time evolution of the orbital Wigner function Eq. (12) can be written as

$$\partial_t w_{\alpha\beta}(\mathbf{x}, \mathbf{k}, t) = \sum_{m=0}^{\infty} \frac{i^{m+1}}{m! 2^m} \sum_{\vec{i} \in \{1, 2, \dots, d\}^m} \sum_{\gamma=1}^M \partial_{x_{\vec{i}}}^{(m)} w_{\alpha\gamma}(\mathbf{x}, \mathbf{k}, t) \partial_{k_{\vec{i}}}^{(m)} h_{\gamma\beta}(\mathbf{k}) - (-1)^m \partial_{k_{\vec{i}}}^{(m)} h_{\alpha\gamma}(\mathbf{k}) \partial_{x_{\vec{i}}}^{(m)} w_{\gamma\beta}(\mathbf{x}, \mathbf{k}, t). \quad (\text{B2})$$

However, the summation over internal indices is just ordinary matrix multiplication, and suppressing matrix indices we can write this more simply as

$$\begin{aligned} \partial_t w(\mathbf{x}, \mathbf{k}, t) &= -i \sum_{m=0}^{\infty} \frac{(-1)^m}{(2m)!2^{2m}} \sum_{\vec{i} \in \{1,2,\dots,d\}^m} [\partial_{k_{\vec{i}}}^{(m)} h(\mathbf{k}), \partial_{x_{\vec{i}}}^{(m)} w(\mathbf{x}, \mathbf{k}, t)] \\ &\quad - \sum_{m=0}^{\infty} \frac{(-1)^m}{(2m+1)!2^{2m+1}} \sum_{\vec{i} \in \{1,2,\dots,d\}^m} \{\partial_{k_{\vec{i}}}^{(m)} h(\mathbf{k}), \partial_{x_{\vec{i}}}^{(m)} w(\mathbf{x}, \mathbf{k}, t)\}. \end{aligned} \quad (\text{B3})$$

We note that whenever $h(\mathbf{k})$ is differentiable, the linear-order term in spatial derivatives in Eq. (B3) only vanishes if all other higher-order terms vanish. Given that ballistic transport, when present, dominates the dynamics, the above formula shows that finite-range, non-interacting, translation-invariant Hamiltonians are either trivially localized or exhibit ballistic transport.

For convenience, we record the first few terms in this expansion:

$$\begin{aligned} \partial_t w(\mathbf{x}, \mathbf{k}, t) &= -i[h(\mathbf{k}), w(\mathbf{x}, \mathbf{k}, t)] - \frac{1}{2} \sum_{a=1}^d \{\partial_{k_a} h(\mathbf{k}), \partial_{x_a} w(\mathbf{x}, \mathbf{k}, t)\} + \frac{i}{8} \sum_{a,b=1}^d [\partial_{k_a} \partial_{k_b} h(\mathbf{k}), \partial_{x_a} \partial_{x_b} w(\mathbf{x}, \mathbf{k}, t)] \\ &\quad + \frac{1}{48} \sum_{a,b,c=1}^d \{\partial_{k_a} \partial_{k_b} \partial_{k_c} h(\mathbf{k}), \partial_{x_a} \partial_{x_b} \partial_{x_c} w(\mathbf{x}, \mathbf{k}, t)\} + \mathcal{O}(\partial_{\mathbf{x}}^4). \end{aligned} \quad (\text{B4})$$

For a single band, the even-order terms vanish and this expression recovers known results on dispersive corrections to free-fermion dynamics [28, 32]. For multiple bands, the second-order term becomes the leading dispersive correction. Note that all higher-order corrections to Eq. (B3), including this second-order term, are time-reversal invariant and therefore do not describe irreversible effects such as diffusion, which is consistent with the microscopic reversibility of the underlying Hamiltonian dynamics.

Appendix C: Extension to electric fields

In this Appendix, we complete the extension to external electrostatic fields discussed in Section II G. Since \hat{V} is diagonal in real space by assumption, we have $i[\hat{V}, \hat{c}_{j\alpha}] = -iV(\mathbf{R}_{j\alpha}) \hat{c}_{j\alpha}$, and it follows by Eq. (38) that

$$i[\hat{V}, \hat{W}_{\alpha\beta}(\mathbf{x}, \mathbf{k})] = i \sum_{j,j' \in \Lambda} \delta_{\text{B}}(\mathbf{x} - \bar{\mathbf{R}}_{jj'}^{\alpha\beta}) (V(\mathbf{R}_{j\alpha}) - V(\mathbf{R}_{j'\beta})) e^{i\mathbf{k} \cdot (\mathbf{R}_{j\alpha} - \mathbf{R}_{j'\beta})} \hat{c}_{j\alpha}^\dagger \hat{c}_{j'\beta}. \quad (\text{C1})$$

Under the summation, we can Taylor expand

$$V(\mathbf{R}_{j\alpha}) - V(\mathbf{R}_{j'\beta}) = (\mathbf{R}_{j\alpha} - \mathbf{R}_{j'\beta}) \cdot \partial_{\mathbf{x}} V(\mathbf{x}) + \mathcal{O}(\partial_{\mathbf{x}}^2 V) \quad (\text{C2})$$

to yield

$$i[\hat{V}, \hat{W}_{\alpha\beta}(\mathbf{x}, \mathbf{k})] = \partial_{\mathbf{x}} V(\mathbf{x}) \cdot \partial_{\mathbf{k}} \hat{W}_{\alpha\beta}(\mathbf{x}, \mathbf{k}) + \mathcal{O}(\partial_{\mathbf{x}}^2 V). \quad (\text{C3})$$

Substituting a non-uniform electrostatic potential $V(\mathbf{R}) = -e\phi(\mathbf{R})$ and following the manipulations of the previous Appendix B then recovers the ballistic-scale transport equation Eq. (39) at leading order in spatial derivatives. Note that the leading term is exact for the simplest case of a uniform electrostatic field \mathbf{E} i.e. $V(\mathbf{R}) = e\mathbf{E} \cdot \mathbf{R}$ and neglecting off-diagonal contributions to \hat{V} .

We next show that subject to these simplifying assumptions, the usual semiclassical prescription for treating Bloch oscillations [8] continues to hold at higher order in spatial derivatives. The first step is to note that in the presence of a static electric field, the exact Heisenberg equation of motion for the Wigner operator Eq. (20) is modified to

$$\begin{aligned} \partial_t \hat{W}_{\alpha\beta}(\mathbf{x}, \mathbf{k}, t) - e\mathbf{E} \cdot \partial_{\mathbf{k}} \hat{W}_{\alpha\beta}(\mathbf{x}, \mathbf{k}, t) &= -i \sum_{\gamma=1}^M \sum_{\mathbf{r} \in \Lambda} \left(t^{\gamma\alpha}(\mathbf{r}) e^{-i\mathbf{k} \cdot \mathbf{r}_{\gamma\alpha}} \hat{W}_{\gamma\beta}(\mathbf{x} + \mathbf{r}_{\gamma\alpha}/2, \mathbf{k}, t) \right. \\ &\quad \left. - t^{\beta\gamma}(\mathbf{r}) e^{-i\mathbf{k} \cdot \mathbf{r}_{\beta\gamma}} \hat{W}_{\alpha\gamma}(\mathbf{x} - \mathbf{r}_{\beta\gamma}/2, \mathbf{k}, t) \right). \end{aligned} \quad (\text{C4})$$

We next define the accelerating-frame Wigner operator $\hat{U}_{\alpha\beta}(\mathbf{x}, \mathbf{k}, t)$ for all time via the relation

$$\hat{W}(\mathbf{x}, \mathbf{k}, t) = \hat{U}(\mathbf{x}, \mathbf{k} + e\mathbf{E}t, t). \quad (\text{C5})$$

Substituting into Eq. (C4) yields

$$\partial_t \hat{U}_{\alpha\beta}(\mathbf{x}, \mathbf{k}, t) = -i \sum_{\gamma=1}^M \sum_{\mathbf{r} \in \Lambda} \left(t^{\gamma\alpha}(\mathbf{r}) e^{-i(\mathbf{k}-e\mathbf{E}t) \cdot \mathbf{r}_{\gamma\alpha}} \hat{U}_{\gamma\beta}(\mathbf{x} + \mathbf{r}_{\gamma\alpha}/2, \mathbf{k}, t) - t^{\beta\gamma}(\mathbf{r}) e^{-i(\mathbf{k}-e\mathbf{E}t) \cdot \mathbf{r}_{\beta\gamma}} \hat{U}_{\alpha\gamma}(\mathbf{x} - \mathbf{r}_{\beta\gamma}/2, \mathbf{k}, t) \right). \quad (\text{C6})$$

Taylor expanding as in the previous Appendix then yields the derivative expansion

$$\begin{aligned} \partial_t \hat{U}_{\alpha\beta}(\mathbf{x}, \mathbf{k}, t) = & \sum_{m=0}^{\infty} \frac{i^{m+1}}{m!2^m} \sum_{\vec{i} \in \{1,2,\dots,d\}^m} \sum_{\gamma=1}^M \partial_{x_{\vec{i}}}^{(m)} \hat{U}_{\alpha\gamma}(\mathbf{x}, \mathbf{k}, t) \partial_{k_{\vec{i}}}^{(m)} h_{\gamma\beta}(\mathbf{k} - e\mathbf{E}t) \\ & - (-1)^m \partial_{k_{\vec{i}}}^{(m)} h_{\alpha\gamma}(\mathbf{k} - e\mathbf{E}t) \partial_{x_{\vec{i}}}^{(m)} \hat{U}_{\gamma\beta}(\mathbf{x}, \mathbf{k}, t). \end{aligned} \quad (\text{C7})$$

Finally defining accelerating-frame Wigner functions $u_{\alpha\beta}(\mathbf{x}, \mathbf{k}, t) = \langle \hat{U}_{\beta\alpha}(\mathbf{x}, \mathbf{k}, t) \rangle$, we deduce the transport equation

$$\begin{aligned} \partial_t u(\mathbf{x}, \mathbf{k}, t) = & -i \sum_{m=0}^{\infty} \frac{(-1)^m}{(2m)!2^{2m}} \sum_{\vec{i} \in \{1,2,\dots,d\}^m} [\partial_{k_{\vec{i}}}^{(m)} h(\mathbf{k} - e\mathbf{E}t), \partial_{x_{\vec{i}}}^{(m)} u(\mathbf{x}, \mathbf{k}, t)] \\ & - \sum_{m=0}^{\infty} \frac{(-1)^m}{(2m+1)!2^{2m+1}} \sum_{\vec{i} \in \{1,2,\dots,d\}^m} \{ \partial_{k_{\vec{i}}}^{(m)} h(\mathbf{k} - e\mathbf{E}t), \partial_{x_{\vec{i}}}^{(m)} u(\mathbf{x}, \mathbf{k}, t) \}. \end{aligned} \quad (\text{C8})$$

Truncating this at leading order in spatial derivatives recovers Eq. (41) of the main text.

Appendix D: Numerical methods

1. Staggered leapfrog method

A real-space numerical scheme that we have found suitable for integrating both Eqs. (21) and its time-dependent generalization (35) numerically is a modification of the standard second-order staggered leapfrog method [53] to include the internal rotation term $-i[h, w]$, which prevents these equations from being in standard flux-conserving form. For simplicity we summarize the details in one spatial dimension, relevant to the plots shown in this paper. We first introduce spatial and temporal grids x_j and t_n with equal spacings Δx and Δt respectively. In the absence of an external potential, the numerical integration can be performed independently for each k -point and is therefore parallelizable. We found that 200 k -points were sufficient to capture the initial charge and charge-current densities in this paper. We also set $\Delta x = 1$ and varied Δt depending on the difficulty of achieving convergence, which we defined for practical purposes as invariance under halving the time step.

To present the scheme, we fix a k -point and use the shorthand $w_j^n = w(x_j, k, t_n)$ for the matrix-valued Wigner function at each spacetime grid point. After the specification of the initial condition $w(x, k, 0)$, we obtain the spatial profile at time $t_1 = \Delta t$ from a Lax Forward Time Centered Space (FTCS) [53] update rule,

$$w_j^1 = \frac{1}{2}(w_{j+1}^0 + w_{j-1}^0) - \frac{\Delta t}{4\Delta x} \{ \partial_k h(k, t), w_{j+1}^0 - w_{j-1}^0 \} - i\Delta t [h(k, t), w_j^0]. \quad (\text{D1})$$

The integration for all subsequent time steps $n > 1$ is carried out using a second-order-staggered-leapfrog-type update rule

$$w_j^{n+1} = w_j^{n-1} - \frac{\Delta t}{2\Delta x} \{ \partial_k h(k, t), w_{j+1}^n - w_{j-1}^n \} - 2i\Delta t [h(k, t), w_j^n]. \quad (\text{D2})$$

2. GPU Fourier Kernel

One of the key computational advantages of the Wigner formalism lies in the “forgotten” information associated with the full density matrix representation. For a box of size $\mathbf{\Lambda} \equiv (\Lambda_0, \Lambda_1, \dots, \Lambda_d)$ and a uniform lattice grid $\mathbf{G} = \mathbf{Z}^d \cap \mathbf{\Lambda}$, the Wigner function as defined in Eq. (12) $w_{\alpha\beta}(\mathbf{x}, \mathbf{k})$ is represented by a tensor with $\mathbf{\Lambda} \cdot \mathbf{\Lambda} M^2$ entries (M is the unit-cell dimension). Note, the same number of entries is required for a full density matrix description on the grid \mathbf{G} , but time evolution operates only on the unit cell versus on the entire density matrix.

For translation invariant non-interacting systems, we can work in the Bloch Hamiltonian basis to effectively reduce the computations of the full density matrix. Indeed, even in the presence of a uniform electric field, the Bloch states are modified as in Appendix C and the savings are shared in both formalisms. However, for non-uniform electric fields (and more generally local potentials), the Wigner formalism can also incorporate them as forcing terms perturbatively as in Eq. (39).

Regardless of method, Wigner or exact-diagonalization (ED), the tensor structure lends itself to a GPU implementation. This is done as follows in PyTorch [93] for the general time-dependent case:

1. Express the Bloch Hamiltonian as a torch.stack of different time and momentum slices, i.e., a tensor representation of the Hamiltonian indexed by time and momentum.
2. Initialize a tensor representation of the initial state using the approximate thermal state in Eq. (25).
3. Fourier transform $\mathbf{x} \rightarrow \mathbf{p}$ via the built in torch.einsum function (allows for custom BZ boundary conditions)—the $\partial_{\mathbf{x}}$ in Eq. (C8) just pulls down an $i\mathbf{p}$.
4. Construct the Fourier Kernel by solving the Wigner equation of motion (C8). Practically, this is done by enlarging the unit cell such that (in 1D) $\mathbf{h}(k) = e^{ik}\mathbf{h}_+ + e^{-ik}\mathbf{h}_- + \mathbf{h}_0$. Then $\partial_k \mathbf{h}(k) = -\partial_k^3 \mathbf{h}(k)$ and $\partial_k^2 \mathbf{h}(k) = -\partial_k^4 \mathbf{h}(k)$. This closes the sum in Eq. (C8), which permits a re-summation of even and odd terms

$$\mathbb{E}_j(\mathbf{p}, \mathbf{k}) = \cos \frac{p}{2} (h_{j+}(k) + h_{j-}(k)) + h_{j0} \quad (\text{D3})$$

$$\mathbb{O}_j(\mathbf{p}, \mathbf{k}) = \sin \frac{p}{2} \partial_k (h_{j+}(k) + h_{j-}(k)) \quad (\text{D4})$$

We can then solve the equation of motion (in the time-independent case) by

$$w(\mathbf{p}, \mathbf{k}, t) = e^{-i\mathbf{h}(\mathbf{k}+\mathbf{p}/2)t} w(\mathbf{p}, \mathbf{k}, 0) e^{i\mathbf{h}(\mathbf{k}-\mathbf{p}/2)t}. \quad (\text{D5})$$

Note: Re-writing the Hamiltonian in the above form allows us to compress the time evolution tensor from $\mathbf{\Lambda} \cdot \mathbf{\Lambda} M^2$ parameters to $2|\mathbf{\Lambda}|M^2$ parameters by interpolating the grids.

5. In the case of a time dependent Hamiltonian $\mathbf{h}(\mathbf{k} \pm \mathbf{p}/2, t)$, we Trotterize the evolution into steps

$$U(t_f, t_0) = \prod_{n=0}^T e^{-\frac{i}{T} \mathbf{h}(\mathbf{k} \pm \mathbf{p}/2, t_0 + (t_f - t_0)n/T)}. \quad (\text{D6})$$

The Trotterization can be instantiated as a torch.stack and grouped into pairs by the associative property of matrix multiplication, i.e. take $T = 2^D$ and pair $\mathbf{h}(t_i), \mathbf{h}(t_{i+1})$ such that

$$\begin{aligned} & \prod_{n=0}^T \exp\left[-\frac{i}{T} \mathbf{h}(\mathbf{k} \pm \mathbf{p}/2, t_0 + (t_f - t_0)n/T)\right] \rightarrow \\ & \prod_{n=0}^{T/2} \exp\left[-\frac{i}{T} \mathbf{h}(\mathbf{k} \pm \mathbf{p}/2, t_0 + (t_f - t_0)2n/T)\right] \exp\left[-\frac{i}{T} \mathbf{h}(\mathbf{k} \pm \mathbf{p}/2, t_0 + (t_f - t_0)(2n+1)/T)\right] \end{aligned} \quad (\text{D7})$$

repeating D times, the tower of tensors collapses to a single tensor over the grid \mathbf{G} of $M \times M$ unitary operators. The exponential reduction in number of time slices is done in batches over the joint \mathbf{p}, \mathbf{k} grid to save memory.

6. The final state is inverse Fourier transformed back via the same torch.einsum operation.

Note, the boundary conditions for Fourier Kernel methods are notoriously difficult to match after numerical integration, e.g., Gibbs phenomena [94]. We avoid this by taking advantage of the enormous system sizes GPU computation permits us to access and simply truncate boundary terms. As a consequence, effects such as Thouless pumping that are sensitive to the boundary are verified using the real-space method of Appendix D 1, but all wave packet dynamics (e.g., in Fig. 6) can be computed far from the boundary.